Remote Sensing of Environment 205 (2018) 151–165

Contents lists available at ScienceDirect

Remote Sensing of Environment

journal homepage: www.elsevier.com/locate/rse

Remote sensing retrievals of colored dissolved organic matter and dissolved organic carbon dynamics in North American estuaries and their margins

Fang Cao[a], Maria Tzortziou[a,*], Chuanmin Hu[b], Antonio Mannino[c], Cédric G. Fichot[d], Rossana Del Vecchio[e], Raymond G. Najjar[f], Michael Novak[c]

[a] Department of Earth and Atmospheric Sciences, The City College of New York, City University of New York, New York, NY 10031, USA
[b] College of Marine Science, University of South Florida, St. Petersburg, FL 33701, USA
[c] NASA Goddard Space Flight Center, Mail Code 616.1, Greenbelt, MD 20771, USA
[d] Department of Earth and Environment, Boston University, Boston, MA 02215, USA
[e] Earth System Science Interdisciplinary Center, University of Maryland, College Park, MD 20740, USA
[f] Department of Meteorology and Atmospheric Science, The Pennsylvania State University, University Park, PA 16802, USA

ARTICLE INFO

Keywords:
Carbon dynamics
CDOM
DOC
MERIS
Estuaries
Coastal
Wetlands
Optics
Biogeochemistry
Tidal exchanges
Extreme precipitation

ABSTRACT

Dissolved organic carbon, DOC, and the colored component of dissolved organic matter, CDOM, are key indicators of coastal water quality and biogeochemical state. Yet applications of space-based remote sensing to monitoring of CDOM variability across estuarine ecosystems and assessment of DOC exchanges along highly dynamic terrestrial-aquatic interfaces have been scarce, in part due to the coarse spatial resolution of most existing ocean color sensors and the seasonal and regional dependence of most existing algorithms. Here, we used a rich dataset of field observations to develop and validate new CDOM and DOC algorithms that are broadly applicable to different estuarine and coastal regions, over different seasons and a wide range of in-water conditions. Algorithms were applied to satellite imagery from MERIS-Envisat at a spatial resolution (300 m) that can resolve much of the spatial variability that characterizes estuaries and their margins. Multi-spectral remote sensing reflectance (R_{rs}) was used to retrieve CDOM absorption at various wavelengths and CDOM absorption spectral slope in the 275–295 nm spectral range ($S_{275–295}$). DOC concentrations were obtained from a tight relationship between the DOC-specific CDOM absorption and $S_{275–295}$, two optical quantities that depend only on the quality of CDOM and strongly covary across spatial and temporal scales. Algorithm evaluation using MERIS satellite data across different estuarine and coastal environments (i.e., the northern Gulf of Mexico, the Delaware Bay, the Chesapeake Bay estuary, and the Middle Atlantic Bight coastal waters) and across different seasons over multiple years resulted in relative errors (mean absolute percent difference; MAPD) of 29% (N = 17), 9.5% (N = 14), and 18% (N = 32), for $a_{CDOM}(300)$, $S_{275–295}$, and DOC, respectively. These relative errors are comparable to those previously reported for satellite retrievals of CDOM and DOC products in less optically complex offshore waters. Application of these algorithms to multi-year MERIS satellite imagery over the Chesapeake Bay estuary allowed, for the first time, to capture the impact of tidal exchanges on carbon dynamics along wetland-estuary interfaces, and resolved spatial gradients, seasonal variability, and year-to-year changes in estuarine carbon amount and quality associated with marsh carbon export, riverine inputs, and extreme precipitation events.

1. Introduction

Estuaries are not only transporters, they are transformers of biogeochemical fluxes between terrestrial and coastal aquatic ecosystems (Bauer et al., 2013; Herrmann et al., 2015). Terrestrial inputs from natural and anthropogenic activities, tidal exchanges with brackish wetlands, atmospheric deposition, rich biodiversity, high in situ primary productivity, photochemistry, and microbial alterations in estuaries result in strong fluxes and extensive transformations of allochthonous and autochthonous organic materials, ultimately controlling the transfer, distribution, and quality of carbon to the coastal ocean (e.g., Bronk, 2002; Cauwet, 2002; Tzortziou et al., 2008). Assessing the impact of estuaries on carbon budgets, however, has been a difficult undertaking due to the tremendous heterogeneity of estuarine systems and the large uncertainties in scaling up in situ observations (Bauer et al., 2013). Synoptic ocean color observations from space provide a

* Corresponding author.
E-mail address: mtzortziou@ccny.cuny.edu (M. Tzortziou).

https://doi.org/10.1016/j.rse.2017.11.014
Received 16 April 2017; Received in revised form 12 October 2017; Accepted 10 November 2017

unique means for scaling up and capturing biogeochemical exchanges across scales and systems (e.g., Balch et al., 2016; Mannino et al., 2016). Yet applications of space-based retrievals to carbon monitoring and, especially, dissolved organic carbon (DOC) dynamics across turbid estuaries remain scarce, in part due to the bio-optical complexity characterizing these highly dynamic nearshore environments (e.g., Le et al., 2013b; Joshi et al., 2017) and the coarse spatiotemporal resolution of most ocean color sensors (Salisbury et al., 2015).

DOC represents over 80–90% of the total organic carbon in the coastal ocean, playing a critical role in a broad range of climate-related biogeochemical cycles (Bates and Hansell, 1999; Hedges, 1992). Characterized as "the great modulator" in aquatic ecosystems (i.e., the variable that modifies the influence of other variables) (Prairie, 2008), DOC and the colored component of dissolved organic matter, CDOM, affect processes such as estuarine ecosystem metabolism, nutrient uptake, the balance between autotrophy and heterotrophy, acidity, bioavailability and toxicity of trace metals and contaminants, photochemical release of biologically labile organic compounds, photoproduction of trace gases, and phytoplankton activity (Benner, 2002; Carlson, 2002; Stanley et al., 2012).

Generally correlating well with DOC in most coastal waters, CDOM absorption properties (e.g., absorption magnitude and spectral slope) have been extensively used as optical proxies to trace DOC dynamics and fingerprint DOM sources in nearshore environments (Asmala et al., 2012; Del Castillo et al., 1999; Del Vecchio and Blough, 2004; Fichot and Benner, 2012; Guéguen et al., 2016; Mannino et al., 2008; Osburn et al., 2016; Spencer et al., 2012; Stedmon et al., 2000; Tzortziou et al., 2015; Vantrepotte et al., 2015). Satellite-derived CDOM absorption and DOC distributions have been used to determine carbon inventories in coastal waters (e.g., Liu et al., 2014) and estimate DOC fluxes across the continental shelf boundary in combination with hydrodynamic models (e.g., Mannino et al., 2016). Most satellite ocean color algorithms of DOC rely on the strong correlation between DOC concentration and CDOM absorption at a specific wavelength λ, $a_{CDOM}(\lambda)$. This correlation, however, varies seasonally and regionally in coastal waters (e.g., Bowers et al., 2004; Del Castillo and Miller, 2008; Mannino et al., 2008). In estuaries and their margins, variability in the CDOM–DOC relationship is also strong across salinity gradients and tidal cycles, due to changes in the source and quality of CDOM (Del Vecchio and Blough, 2004; Tzortziou et al., 2008; Tzortziou et al., 2011).

Spectral CDOM absorption properties (spectral slope, S, and slope ratios) have been previously used as indicators of the source, molecular weight, aromatic content, photobleaching and microbial alteration of CDOM in estuarine and coastal environments (Chin et al., 1994; Green and Blough, 1994; Belzile and Guo, 2006; Helms et al., 2008). Alternative remote sensing algorithm approaches have therefore been proposed to obtain DOC concentrations using satellite estimates of both CDOM absorption magnitude and spectral slope in coastal waters (e.g., Fichot et al., 2014; Mannino et al., 2016). Most of these approaches have been applied to moderate spatial resolution (e.g., 0.75–1 km at nadir) satellite imagery from sensors such as SeaWiFS, MODIS, and VIIRS, which are not optimal for application in small and highly heterogeneous nearshore environments. Undersampling of spatial variability can have a significant effect on the products derived from satellite imagery (Mouw et al., 2015). Lee et al. (2012) demonstrated that coarse spatial resolution (1.2-km reduced resolution relative to 300-m full resolution MERIS imagery) can lead to underestimates in derived biogeochemical properties of the target area. Satellite observations from high spatial resolution sensors such as the Landsat-8 Operational Land Imager have been used for CDOM retrievals in estuaries (e.g., Slonecker et al., 2016). However, the limited number of spectral bands on these sensors is not ideal for retrieving the spectral shape of CDOM absorption, and the 16-day revisit time is not optimal for monitoring processes in very dynamic coastal systems.

Given these challenges in satellite retrievals of CDOM and DOC in optically complex coastal waters, the objective of this study was to develop and test new algorithms that, first, are more broadly applicable across different estuarine environments and seasons and, second, use multi-spectral satellite imagery at a spatial resolution that can resolve much of the spatial variability that characterizes estuaries and their margins. With a 300-m spatial resolution (full resolution data), 2-day revisit frequency, and 9 spectral bands (412–710 nm) for ocean color, the Medium Resolution Imaging Spectrometer (MERIS, 2002–2012) has been shown to be particularly effective in resolving spatial gradients in nearshore biological processes, including capturing coastal water quality dynamics (Le et al., 2016), assessing changes in chlorophyll in estuarine upwelling systems (Spyrakos et al., 2011), and detecting harmful algal blooms in estuaries and lakes (e.g., Lunetta et al., 2015). Here, we used full-resolution (300-m) MERIS imagery to develop new CDOM and DOC algorithms that were evaluated, for the first time, across estuarine systems using satellite and in situ match-ups spanning different seasons and multiple years. Results were compared with 1-km resolution MODIS retrievals. In our approach, multi-spectral remote sensing reflectance (R_{rs}) is used to retrieve both CDOM absorption and the CDOM absorption spectral slope in the 275–295 nm spectral range ($S_{275–295}$). DOC concentrations are then obtained from a tight relationship between the DOC-specific CDOM absorption and $S_{275–295}$, two optical quantities that depend only on the quality of DOM. This approach allows for a broader application across coastal regions and temporal scales. The algorithms were developed and evaluated using field measurements and satellite observations from the northern Gulf of Mexico, the Chesapeake Bay, and the Delaware Bay estuaries in the United States, and were implemented to assess impacts of extreme events (e.g., tropical storms) on estuarine CDOM and DOC dynamics from space-based observations. Observed patterns are discussed with a particular focus, for the first time, on highly dynamic biogeochemical processes and exchanges in tidally influenced wetland-estuarine interfaces.

2. Study area

The study region used to develop and evaluate the CDOM and DOC algorithms encompassed three large estuarine–coastal systems in the United States: the Chesapeake Bay and Delaware Bay estuaries, the adjacent coastal waters of the Middle Atlantic Bight, and the northern Gulf of Mexico (Fig. 1 and Table 1).

2.1. Chesapeake Bay

The Chesapeake Bay, along with its tidal tributaries, is the largest and most productive estuary in the nation. The Bay is approximately 320 km long from the mouth of the Susquehanna River in the north to its outlet into the Middle Atlantic Bight in the south. The Bay's width ranges from 6 km near Aberdeen, Maryland, to 48 km near Cape Charles, Virginia, while its average depth, including all tidal tributaries, is 6.4 m (https://www.chesapeakebay.net). Primary productivity, nutrient concentrations, and distributions of suspended particles and dissolved organic substances are highly variable in the Chesapeake Bay, and are influenced by freshwater inputs from rivers and wetlands, frontal features and tides, and lateral gradients driven by estuarine circulation (Adolf et al., 2006; Harding, 1994; Hood et al., 1999; Tzortziou et al., 2008). The estuarine circulation results in relatively long and variable residence times (90 to 180 days) for freshwater and nutrients (Kemp et al., 2005).

2.2. Delaware Bay

The Delaware Bay is another large and turbid estuary off the Middle Atlantic Bight (Sharp et al., 2009). It features an upper 100-km long tidal portion of the Delaware River and a lower 120-km long saline portion, with a turbidity maximum zone that lies in between these two segments. The tidal Delaware River runs from the head of tide at

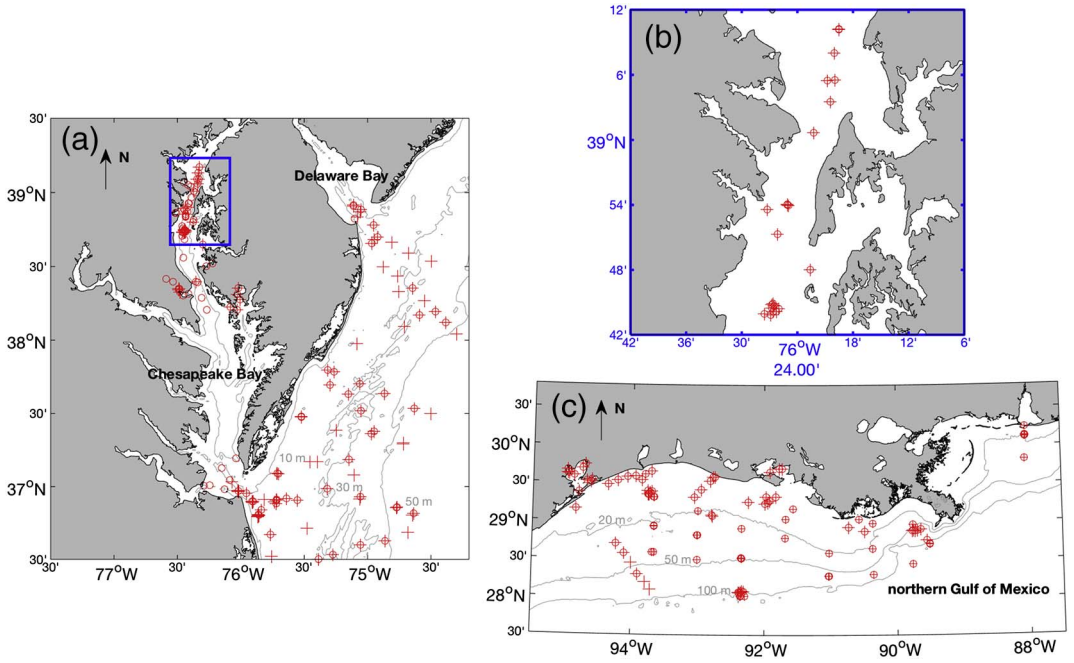

Fig. 1. Sampling locations for the training data set, including: (a) the Chesapeake Bay, Delaware Bay, and coastal Mid-Atlantic Bight waters, with (b) providing a closer look at the location of sites in the upper Chesapeake Bay, and (c) the northern Gulf of Mexico. Coincident R_{rs} and a_{CDOM} measurements are shown by plus symbols (N = 234) and coincident a_{CDOM} and DOC measurements are shown by open circles (N = 250).

Trenton, NJ, through the greater Philadelphia, PA area, influenced by freshwater tidal wetlands and heavy loadings of anthropogenic carbon and nutrients (Harvey and Mannino, 2001; Mannino and Harvey, 1999; Mannino and Rodger, 2004). The lower Delaware Bay is a large shallow embayment surrounded by partially undeveloped salt marshes (Sharp et al., 2009). Overall the Delaware Bay is dynamically controlled by interactions between a river-dominated upper estuary and a coastal influenced lower bay.

2.3. Northern Gulf of Mexico

The northern Gulf of Mexico is a river-dominated coastal system. The Mississippi and Atchafalaya Rivers contribute > 80% of the total freshwater input to this coastal region, whereas the remaining 20% comes primarily from other smaller rivers and estuaries in Louisiana (Lohrenz et al., 2008). Estuaries along the northern Gulf of Mexico coast are generally shallow, and experience weak tides relative to the Chesapeake and Delaware Bay. The Gulf of Mexico estuarine shorelines are highly indented with river inlets, deltas, as well as extensive tidal fresh and brackish marshes (Das et al., 2012; Gibson and Najjar, 2000; Kemp et al., 2014). Excess nutrients from the Mississippi River and seasonal stratification of waters in the Gulf make the region off the coast of Louisiana and Texas the largest bottom-water hypoxic zone in the United States and the second largest in the world (www.gulfhypoxia.net, Rabalais et al., 2002).

Table 1
List of field measurements used for algorithm development.

Cruises	Region	Dates	Paired measurements		Data source (investigators)	
			Rrs & CDOM	CDOM & DOC	*Rrs*	CDOM & DOC
GEO-CAPE_GoMEX	Northern Gulf of Mexico	September 9–22, 2013	57	60	SeaBASS (Z. Lee & M. Ondrusek)	SeaBASS (A. Mannino)
GEO-CAPE_CBODAQ	Chesapeake Bay main stem	July 7–22, 2011	40	40	SeaBASS (C. Hu)	SeaBASS (A. Mannino)
	Blackwater Refuge Marshes and adjacent estuarine water		4	4	SeaBASS (S. Hooker)	SeaBASS (M. Tzortziou)
GulfCarbon	Northern Gulf of Mexico	Seasonally, 2009–2010	49	49	Fichot et al. (2014)	
Bio_optics_Chl_polarization	Upper Chesapeake Bay main stem and bay mouth	August 12–22, 2013	36	n.a.[a]	SeaBASS (A. Gilerson)	SeaBASS (M. Tzortziou)
Chesapeake_Bay_Plume_D01	Chesapeake Bay mouth and bay plume	May 27, 2005	n.a. [a]	4	Mannino et al. (2008)	
Chesapeake_Bay_Plume_D03		September 6, 2006	2	5		
Chesapeake_Bay_Plume_D04		November 28, 2006	3	6		
BIOME_B01	Coastal waters at the shelf of the Mid-Atlantic Bight	March 30–April 1, 2005	6	15		
BIOME_B02		July 26–31, 2005	16	26		
BIOME_B03		May 9–12, 2006	n.a.[a]	10		
BIOME_B04		July 2–6, 2006	21	31		

[a] n.a. DOC or R_{rs} not available.

Table 2
Satellite match-ups used for algorithm validation.

Cruises	Region	Dates	MODIS		MERIS		Data source (investigators)
			CDOM	DOC	CDOM	DOC	
GEO-CAPE_GoMEX	Northern Gulf of Mexico	September 9–22, 2013	4	4	n.a.	n.a.	SeaBASS (A. Mannino; M Tzortziou)
GulfCarbon	Northern Gulf of Mexico	Seasonally 2009–2010	16	16	6	6	Fichot et al. (2014)
Bio_optics_Chl_polarization	Upper Chesapeake Bay main stem and bay mouth	August 12–22, 2013	2	2	n.a.	n.a.	SeaBASS (A. Gilerson; M. Tzortziou)
Chesapeake_Bay_Plume_D02	Chesapeake Bay mouth and bay plume	November 3, 2005	6	6	5	5	Mannino et al. (2008)
BIOME_B02	Coastal waters at the shelf of the Mid-	July 26, 2005	1	1	n.a.	n.a.	
BIOME_B03	Atlantic Bight	May 11–12, 2006	7	7	n.a.	n.a.	
BIOCOMP0302	Chesapeake Bay main stem, upper bay	October 3–4, 2003	3	n.a.	1	n.a.	SeaBASS
MOVE0803	to bay mouth	August 23, 2003	2	n.a.	n.a.	n.a.	(L. Harding, M. Mallonee, & A.
SGER1103	Chesapeake Bay main stem, nearshore	November 10, 2003	3	n.a.	2	n.a.	Magnuson)
Delaware Bay Cruises	Delaware River and Estuary	April, September, October, December 2006	n.a.	14	na	20	R. Del Vecchio
Delaware River and Estuary		March, October 2011	n.a.	3	na	1	McIntosh (2013)
EN372	Delaware Bay	July 1–3, 2002	n.a.	n.a.	3[a]	n.a.	SeaBASS (R. Morrison & H. Sosik)

[a] Three samples of EN372 contain data only of $a_{CDOM}(300)$.

3. Data and methods

3.1. In situ datasets for algorithm development and evaluation

To develop and evaluate the CDOM and DOC algorithms, we synthesized field observations in the Chesapeake Bay, the Delaware Bay, and the northern Gulf of Mexico obtained from the SeaWiFS Bio-optical Archive and Storage System (SeaBASS) and other datasets contributed by individual investigators (Tables 1 and 2) (Fichot et al., 2014; Mannino et al., 2008; McIntosh, 2013). The assembled dataset contained coincident measurements of remote-sensing reflectance spectra, $R_{rs}(\lambda)$, and CDOM absorption spectra, $a_{CDOM}(\lambda)$, in the UV–visible spectral regions (λ = 270–750 nm), and coincident measurements of $a_{CDOM}(\lambda)$ and DOC concentrations. The CDOM absorption spectral slope coefficient in the 275–295 nm spectral region ($S_{275–295}$, nm^{-1}) was calculated as the slope of the linear regression of the logarithm of $a_{CDOM}(\lambda)$ over 275–295 nm (Helms et al., 2008). The resulting dataset included measurements collected during different seasons and years for different salinity ranges along the river–estuary–coastal ocean continuum.

The compiled dataset was split into two subsets, one used for training and development of the algorithms and the other used for evaluation. To maximize the number of field–satellite data matchups, in situ measurements of R_{rs}, CDOM, and DOC with no concurrent satellite overpasses were used to develop the algorithms, while field measurements that could be matched with corresponding satellite R_{rs} were included into the evaluation dataset to evaluate the performance of the algorithms. No data from the algorithm development was used in the evaluation.

3.2. Satellite data and processing

Satellite ocean color data used in this study were from the Medium Resolution Imaging Spectrometer (MERIS) on Envisat-1 platform and the Moderate Resolution Imaging Spectroradiometer onboard the Aqua satellite (MODIS-A). MERIS and MODIS-A data were obtained from the NASA Ocean Biology Distributed Active Archive Center (OB-DAAC; https://oceancolor.gsfc.nasa.gov) and processed using the SeaWiFS Data Analysis System (SeaDAS, 7.3.1).

The algorithm was applied to Level-2 R_{rs} data from MODIS-A at a 1-km nadir resolution (data processing version R2014.0) and full resolution (FRS, 300 m at nadir) Level-2 R_{rs} data from MERIS (data processing version R2012.1), over a period from July 2002 to September 2013 (Table 2). Level-2 1-km resolution R_{rs} from MODIS and full resolution R_{rs} from MERIS for February 2011 were spatially binned at their nominal resolution to generate Level-3 products that were used to highlight the improved spatial coverage obtained by the higher spatial resolution MERIS imagery compared to MODIS. To examine seasonal patterns and the impacts of extreme weather events (e.g., storms) on CDOM and DOC dynamics in the Chesapeake Bay, subsets of Level-2 full resolution MERIS ocean color R_{rs} data over the Chesapeake Bay were created for normal weather conditions during January to December 2009, and also for October 2011 when tropical storm Lee impacted this area. Level-3 monthly R_{rs} composites were produced using default settings in SeaDAS. Wavelength discrepancies between the two sensors were overcome by linearly interpolating MERIS R_{rs} to corresponding MODIS wavelengths prior to algorithm evaluation and application to MERIS.

3.3. Algorithm development using in situ data

3.3.1. Development of CDOM algorithms

A number of remote sensing algorithms have been developed over the past two decades to retrieve CDOM absorption from ocean color observations (e.g., Carder et al., 1999; Lee et al., 2010; Lee et al., 2002; Siegel et al., 2005; Werdell et al., 2013). In most of these retrievals, CDOM and non-algal particulate (NAP) absorption are estimated as a single parameter because of their similar absorption spectral shape. Other algorithms, that simultaneously retrieve CDOM, NAP, and phytoplankton, are often based on assumptions and parameterizations (e.g., constant absorption spectral slopes for CDOM and NAP absorption) that are not applicable to highly dynamic estuarine environments (e.g., Magnuson et al., 2004; Maritorena et al., 2002; Morel and Gentili, 2009). Here we used multi-spectral remote sensing reflectance (R_{rs}) measurements to retrieve information on both CDOM absorption magnitude and CDOM absorption spectral slope (e.g., Mannino et al., 2014; Mannino et al., 2016).

To develop the CDOM algorithms, a number of approaches were evaluated to find the best correlation between R_{rs} and a_{CDOM} or $S_{275–295}$ in the training data set. These included both the linear and nonlinear band-ratio methods, as well as a multiple linear regression (MLR) approach. $R_{rs}(412)$ was not used in the algorithm development, because of the higher uncertainty in atmospheric correction in this spectral region especially in nearshore waters close to urban areas (Ahmad et al., 2007). In the conventional band ratio algorithms, various measured in situ R_{rs} band ratios (e.g., $R_{rs}(488)/R_{rs}(555)$, $R_{rs}(488)/R_{rs}(667)$, $R_{rs}(443)/R_{rs}(555)$, etc.) were correlated to the measured in situ a_{CDOM} or $S_{275–295}$ to find the best correlation, evaluated by estimating the

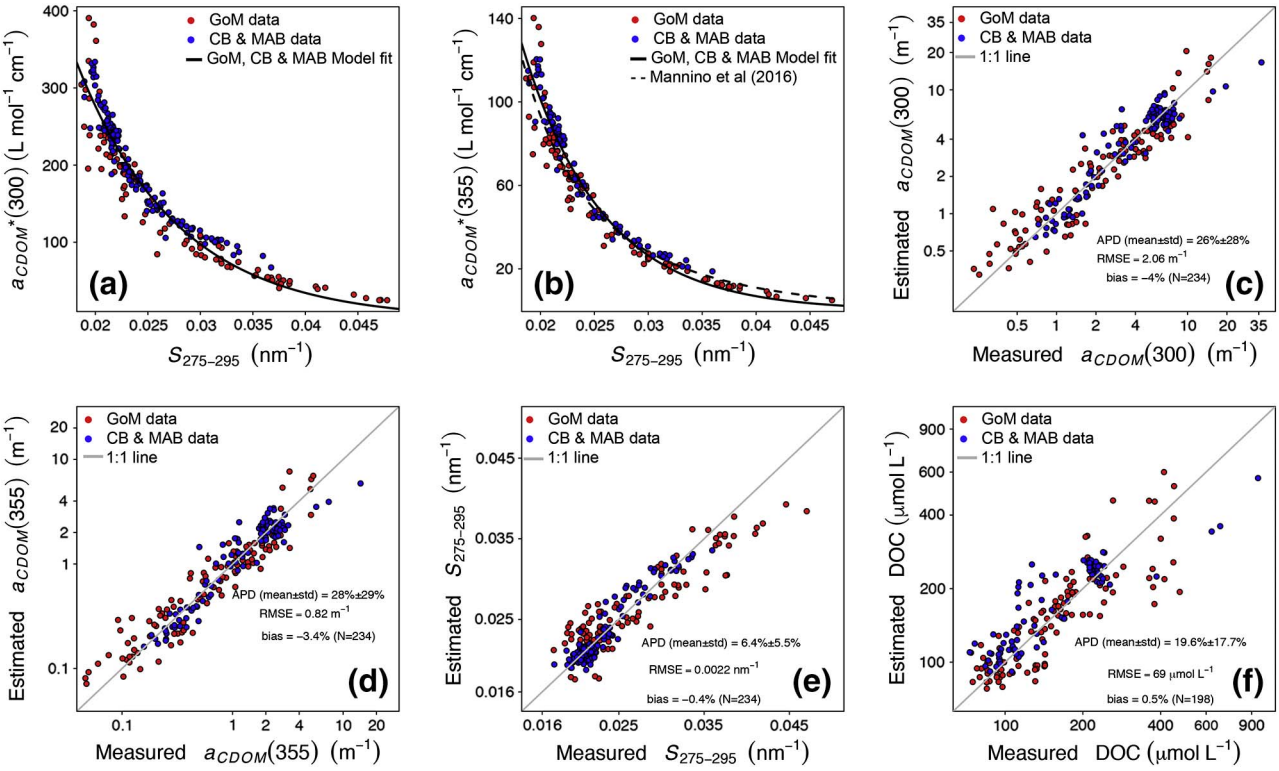

Fig. 2. Relationship between (a) $a_{CDOM}^{*}(300)$ and $S_{275–295}$, and (b) $a_{CDOM}^{*}(355)$ and $S_{275–295}$ for the combined dataset in the Gulf of Mexico (GoM), Chesapeake Bay (CB) and Mid Atlantic Bight (MAB). A comparison with the $a_{CDOM}^{*}(355)$ - $S_{275–295}$ relationship for the continental shelf waters extending from south of Cape Hatteras to south of Cape Cod near Georges Bank discussed in Mannino et al. (2016) is provided in (b). Estimated versus measured (c) $a_{CDOM}(300)$, (d) $a_{CDOM}(355)$, (e) $S_{275–295}$, and (f) DOC.

mean absolute percent difference between measured and estimated parameters (see Section 3.4). The best MLR between $R_{rs}(\lambda)$ at multiple wavelengths and a_{CDOM} was found using a stepwise backward elimination method based on Akaike's Information Criterion (AIC) when the lowest AIC was achieved.

Measured R_{rs} spectra were used to retrieve a_{CDOM} at various wavelengths. The relative error (mean absolute percent difference; MAPD) between retrieved and measured CDOM absorption values using the MLR approach was very similar across the 300–412 nm spectral region (see 4.1). Results are shown in Fig. 2 at 300 nm and 355 nm because of the significantly better signal-to-noise ratio of field measurements of CDOM absorption at shorter wavelengths and because these are reference wavelengths commonly used in studies of CDOM dynamics and photobiogeochemical processes across aquatic environments from coastal to open ocean waters (e.g., Nelson et al., 1998; Del Castillo et al., 1999; Kahru and Mitchell, 2001; Osburn and Stedmon, 2011; Fichot and Benner, 2012; Mannino et al., 2014).

3.3.2. Development of the DOC algorithm

While DOC concentration has been shown to be strongly correlated with CDOM absorption in most estuarine and coastal waters, the relationship between these two parameters is expected to vary temporally and spatially, reflecting the strong variability in the source and quality of CDOM in nearshore environments (Del Vecchio and Blough, 2004; Fichot and Benner, 2011; Mannino et al., 2016). To develop an algorithm that is broadly applicable across various highly dynamic estuarine systems, we assessed the relationship between the DOC-specific CDOM absorption coefficient ($a_{CDOM}^{*}(\lambda)$, defined as the ratio of $a_{CDOM}(\lambda)$ to DOC, in units of L mol^{-1} cm^{-1}) and $S_{275–295}$, two optical quantities that depend on the chemical composition, source, and quality (but not the amount) of CDOM. The derived relationship is presented in Section 4.1.

3.4. Algorithm evaluation and assessment

To evaluate the performance of the developed CDOM and DOC algorithms, we compared field measurements of a_{CDOM}, $S_{275–295}$, and DOC to retrieved parameters using both field and satellite measurements of R_{rs} (Tables 1 and 2). For the satellite validation, the following procedures were carried out to ensure high-quality satellite–in situ match-ups:

1) Satellite level-2 R_{rs} was matched in time with field observations. To obtain a sufficient number of match-ups, the time window between satellite overpass and field sampling was relaxed to ± 24 h, following Le et al. (2013a).
2) A 3 × 3 pixel array centered on the in situ sampling location was extracted to examine the spatial homogeneity. Masks were applied to pixels within the extracted pixel array if any of the following flags were set: atmospheric correction failure, land, sun glint, cloud or ice, high top-of-atmosphere radiance, low normalized water-leaving radiance at 555 nm, and stray light, according to Bailey and Werdell (2006). The only match-ups used for evaluation were those where the number of valid pixels (i.e., after flags) was > 4 and the coefficients of variation for R_{rs} at 488, 531, and 555 nm were < 0.2 within the 3 × 3 pixel array (Mélin et al., 2011).
3) Satellite $a_{CDOM}(300)$, $S_{275–295}$, and DOC were retrieved by implementing the algorithms and a median value of valid pixels in the 3 × 3 pixel array was calculated to discount any potential errors caused by outliers (Hu et al., 2001).

The evaluation of algorithm performance was based on statistical parameters, including the standard deviation of the absolute percent difference (APD), the mean absolute percent difference (MAPD), the root mean square error (RMSE), and the bias defined as follows:

$$\text{mean APD (MAPD)} = \left\{ \sum \left| \frac{[X_i^{estimated} - X_i^{measured}]}{X_i^{measured}} \right| \right\} \times 100/N \quad (1)$$

$$\text{RMSE} = \left\{ \frac{\sum [X_i^{estimated} - X_i^{measured}]^2}{N} \right\}^{\frac{1}{2}} \quad (2)$$

$$\text{bias (\%)} = \left\{ \frac{\frac{1}{N} \times \Sigma (X_i^{estimated} - X_i^{measured})}{mean(X_i^{measured})} \right\} \times 100 \quad (3)$$

where $X_i^{measured}$ and $X_i^{estimated}$ are measured in situ a_{CDOM}, $S_{275–295}$, or DOC values and their corresponding estimates retrieved from the algorithms for the ith observation, respectively. N is the number of observations.

4. Results and discussion

4.1. CDOM and DOC algorithms: development, performance, and evaluation

The MLR approach outperformed the band-ratio approach using our training dataset. In terms of MAPD, relating various band ratios to field measurements of $a_{CDOM}(300)$ gave errors larger than 30%, compared to an error of 26% using MLR. The best regressions using the band-ratio approach were derived by relating $a_{CDOM}(300)$ to $R_{rs}(488)/R_{rs}(555)$ for linear correlation and to $R_{rs}(443)/R_{rs}(555)$ for nonlinear correlation, with errors of 31% and 40%, respectively. For the MLR approach, the R_{rs} at multiple wavelengths determined using the stepwise backward elimination method resulted in an inclusion of five bands for the algorithm, with an AIC of 143.8, compared to AICs of > 150 if more bands were included. Thus, we decided to use the MLR approach to estimate a_{CDOM} and $S_{275–295}$ from ocean color R_{rs} (Eqs (4)–(5)). CDOM algorithms are reported here at both 300 nm and 355 nm (qualitatively similar results for 412 nm, not shown here), for comparison with other studies.

$$\ln(a_{CDOM}(\lambda)) = \alpha \times \ln(Rrs(443)) + \beta \times \ln(Rrs(488)) + \gamma \times \ln(Rrs(531)) + \delta \times \ln(Rrs(555)) + \varepsilon \times \ln(Rrs(667)) + \zeta \quad (4)$$

where:

$\alpha = -0.0206$, $\beta = -0.6128$, $\gamma = -0.0070$, $\delta = -0.4944$, $\varepsilon = 0.9362$, and $\zeta = 0.9666$, $N = 234$, for $\lambda = 300$ nm, and

$\alpha = 0.0376$, $\beta = -0.8714$, $\gamma = -0.0352$, $\delta = -0.2739$, $\varepsilon = 0.9591$, and $\zeta = -0.1071$, $N = 234$, for $\lambda = 355$ nm,

$$\ln(S_{275–295}) = \alpha \times \ln(Rrs(443)) + \beta \times \ln(Rrs(488)) + \gamma \times \ln(Rrs(531)) + \delta \times \ln(Rrs(555)) + \varepsilon \times \ln(Rrs(667)) + \zeta \quad (5)$$

where:

$\alpha = -0.0537$, $\beta = 0.2689$, $\gamma = 0.1017$, $\delta = -0.2097$, $\varepsilon = -0.0893$, and $\zeta = -3.6853$, $N = 234$.

For the DOC algorithm, we examined the relationship between $a_{CDOM}^*(\lambda)$ (at both 300 nm and 355 nm) and $S_{275–295}$ (Fig. 2(a)–(b)). A tight relationship (Pearson R of 0.92 and 0.97 for $a_{CDOM}^*(300)$ and $a_{CDOM}^*(355)$, respectively, $N = 250$, $p < 0.001$) was found between the two quantities using our training dataset that covers different seasons, years, estuaries, and sampling locations across the salinity gradient from the tidal marsh - estuarine interface, to nearshore, estuarine and continental shelf waters. High DOC-specific CDOM absorption values were associated with low $S_{275–295}$, in agreement with previous studies across a range of environments that discussed the use of $S_{275–295}$ as a tracer of the natural variations in $a_{CDOM}^*(\lambda)$ (e.g., Fichot and Benner, 2012; Vantrepotte et al., 2015; Mannino et al., 2016).

In our dataset, applying different MLR retrievals to measurements from distinct coastal regions did not affect significantly the algorithm coefficients or goodness of fit parameters (Pearson coefficients, R, of 0.94 and 0.94, compared to 0.92, when different fits were applied to data from the Gulf of Mexico, and Chesapeake Bay Estuary/Mid-Atlantic Bight, respectively, in the $a_{CDOM}^*(300)$ vs $S_{275–295}$ relationship, Fig. 2(a)). These results suggest that a single, regionally independent algorithm can be applied to these measurements without a significant impact on retrieval accuracy. Similarly, we found that the relationship between $a_{CDOM}^*(\lambda)$ and $S_{275–295}$ in our broad dataset is consistent with algorithms reported in previous studies for distinct coastal regions (e.g., Fichot and Benner, 2012) and higher salinity, more offshore waters (e.g., Mannino et al., 2016; Fig. 2(b)).

The following non-linear regression provided the best fit over the entire range of DOC (73–953 μmol L^{-1}):

$$a_{CDOM}^*(300) = (exp(-15.05 - 33.95 \times S_{275–295}) + exp(-1.502 - 104.3 \times S_{275–295})) \quad (6a)$$

This relationship facilitated the retrieval of DOC concentration from satellite-based retrievals of $a_{CDOM}(300)$ and $S_{275–295}$:

$$\text{DOC} = a_{CDOM}(300)/(exp(-15.05 - 33.95 \times S_{275–295}) + exp(-1.502 - 104.3 \times S_{275–295})) \quad (6b)$$

Units of DOC, $a_{CDOM}(300)$, and $S_{275–295}$ are μmol L^{-1}, m^{-1}, and nm^{-1}, respectively.

Comparisons between field measurements of $a_{CDOM}(\lambda)$ and $S_{275–295}$ with estimates derived from measured in situ $R_{rs}(\lambda)$ spectra using our bio-optical algorithms (Eq. (4) and Eq. (5)), showed very good agreement (Fig. 2(c)–(e)). The algorithms resolved a_{CDOM} across more than two orders of magnitude (e.g., $a_{CDOM}(300)$ in the range of 0.2–37 m^{-1}) with a relative error (MAPD) of 26% and 28.3% at 300 nm and 355 nm, respectively ($N = 234$) (Fig. 2(c)–(d)). A similar MAPD of 26.9% was estimated for CDOM retrievals at 412 nm, (results not shown here). An MAPD value of < 7% (with an RMSE of 0.0022 nm^{-1} and a bias of − 0.4%, $N = 234$) was found for $S_{275–295}$, across a wide range of absorption spectral slope coefficients, from 0.0173 to 0.047 nm^{-1} (Fig. 2(e)). Retrievals of DOC concentrations from measured in situ R_{rs} also demonstrated good agreement with field observations, with an MAPD of < 20%, (RMSE = 69 μmol L^{-1}, bias = 0.5%, $N = 198$) for DOC values ranging from 73 to 953 μmol L^{-1} (Fig. 2(f)).

Algorithm evaluation using satellite R_{rs} showed that the MAPD values for $a_{CDOM}(300)$, $S_{275–295}$, and DOC retrievals were 36%, 8.8%, and 33%, respectively for MODIS-A, and 29%, 9.5%, and 18%, respectively for MERIS (Fig. 3(c–e)). Note that for the evaluation of these algorithms we used satellite data across different estuarine and coastal environments (i.e., the northern Gulf of Mexico, the Delaware Bay, and the Chesapeake Bay estuary), and different seasons over multiple years (Table 2). Still, the DOC retrievals did not show any seasonal or regional dependence (Fig. 3(e)). Although the training dataset used to develop the algorithms contained measurements from the mouth of Delaware Bay, it did not include data from the main stem of the estuary. Nonetheless, the satellite-retrieved DOC concentrations remained in good agreement with field observations across the salinity gradient in the Delaware Bay estuary (Fig. 3), showing the potential of our ocean-color algorithms for synoptic carbon studies across different estuarine environments.

In addition to the inherent uncertainty of the algorithms, several factors can explain some of the observed differences between satellite derived values and in situ measurements (a_{CDOM}, $S_{275–295}$, and DOC). The time difference between the satellite overpass and in-situ observations introduces some uncertainty in the validation of remote sensing retrievals in highly dynamic coastal waters. In our approach, the matchup time window was relaxed to ± 24 h in order to have an evaluation dataset large enough for robust statistical analyses. To assess the impact of time difference between the satellite overpass and in situ observations, validation match-ups for our CDOM algorithms were divided into two groups, match-ups with a ± 0–12 h and a ± 12–24 h

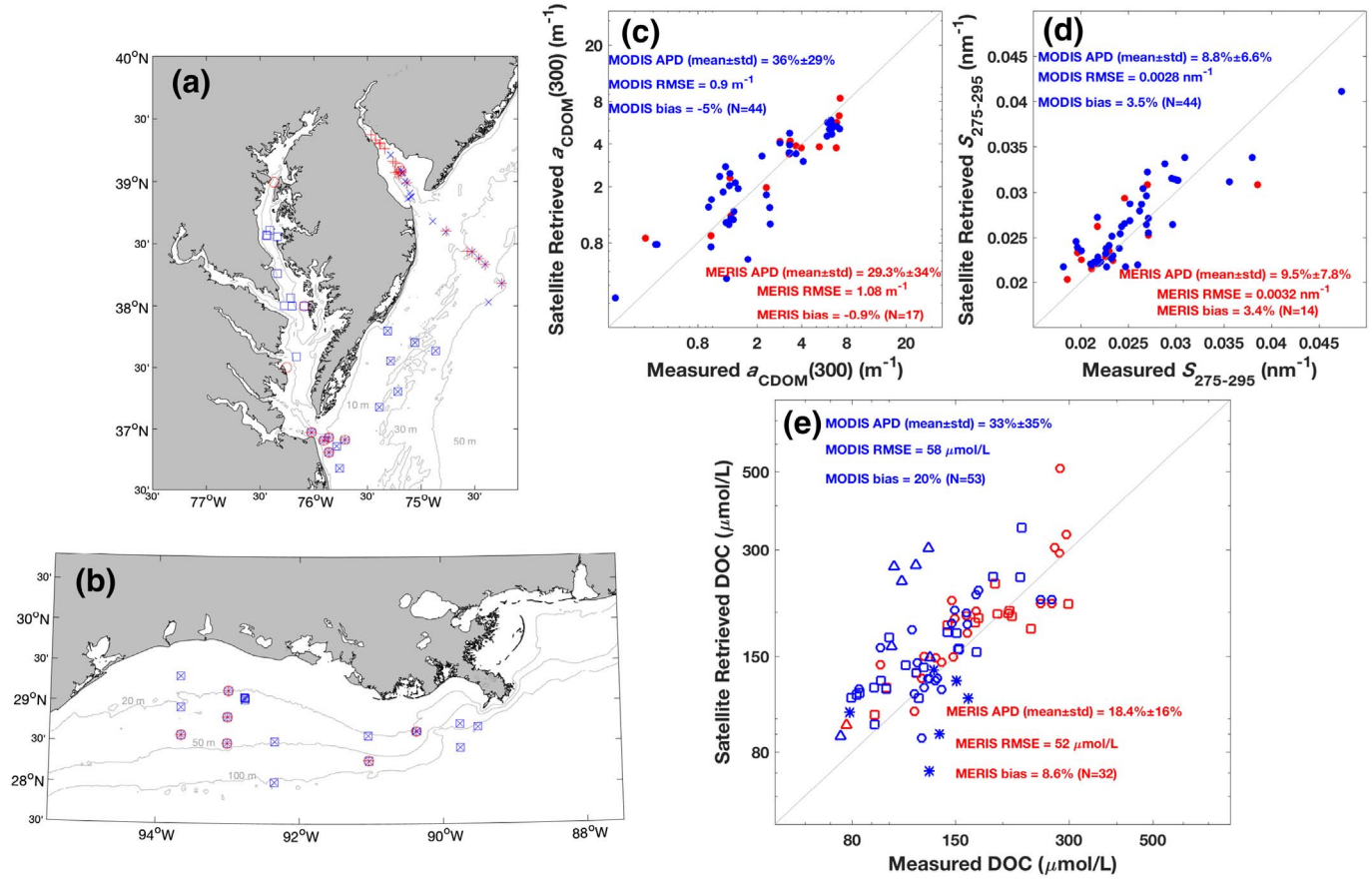

Fig. 3. Evaluation data set (a) in the Chesapeake and Delaware Bay, and (b) in the northern Gulf of Mexico. Different symbols show CDOM matchups with MODIS (blue squares, □) and MERIS (red circles, ○), and DOC matchups with MODIS (blue cross, ×) and MERIS (red plus, +). Satellite retrieved versus measured (c) $a_{CDOM}(300)$, (d) $S_{275–295}$, and (e) DOC, for MODIS (blue) and MERIS (red). In (e) different symbols correspond to different seasons, spring (square), summer (asterisk), fall (circle) and winter (triangle). (For interpretation of the references to color in this figure legend, the reader is referred to the web version of this article.)

time window (data not shown here). No statistically significant differences in the algorithm performance were found between the two groups, which could be due to the superimposed impacts of higher frequency (e.g., hourly) variability, associated with processes such as semi-diurnal tidal biogeochemical exchanges, on estuarine DOC and CDOM dynamics (see discussion in 4.4). Another source of uncertainty is the spatial heterogeneity of these waters affecting comparisons between in situ measurements made at point locations and satellite observations over the much larger satellite footprint. This spatial heterogeneity may potentially explain the overall improved statistics yielded from the 300-m full resolution MERIS match-ups compared to the coarser 1-km MODIS-A imagery (Fig. 3(c–e)). Although many of the nearshore regions included in our study are shallow, they are also carbon-rich and sediment-rich optically deep waters. Thus, bottom reflectance would not be expected to have a large impact on our satellite retrievals, although it would be a source of uncertainty for satellite retrievals in less turbid shallow waters. In addition, atmospheric correction of remotely-sensed ocean reflectance is challenging in nearshore areas, especially in the blue spectral region (i.e., 412 and 443 nm bands) (Ahmad et al., 2007; Goyens et al., 2013). In our retrievals, we did not include $R_{rs}(412)$ and we used the iterative NIR atmospheric correction approach (Bailey et al., 2010) that has been reported to have a reasonable performance in other nearshore turbid environments (e.g., Joshi et al., 2017). Uncertainties in atmospheric correction, due to strong variability in atmospheric aerosol and trace gas amounts, especially in urban coastal regions, could have an impact on the accuracy of our CDOM and DOC retrievals (Tzortziou et al., 2014).

Despite these challenges in nearshore estuarine environments, the relative errors we obtained here for the satellite CDOM and DOC products are comparable to those previously reported for satellite retrievals using a similar MLR approach in less optically complex, further offshore waters. Mannino et al. (2014) and Mannino et al. (2016) reported MAPD values on the order of 24%, 8.7%, and 17–19% for $a_{CDOM}(355)$, $S_{275–295}$, and DOC retrievals, respectively, along the continental shelf of the northeastern United States. Using a quasi-analytical approach, and an evaluation dataset that included measurements in the South China Sea and the Taiwan Strait, Dong et al. (2013) reported an MAPD of 45% for $a_{CDOM}(443)$. Linking CDOM absorption to estimates of the vertical attenuation coefficient, K_d, Loisel et al. (2014) retrieved $a_{CDOM}(412)$ from SeaWiFS R_{rs} and reported an MAPD value of 37% over two orders of magnitude (from 0.01 to 0.98 m^{-1}).

4.2. Applicability of the algorithms

The use of multiple spectral bands in our MLR approach, rather than a single spectral band ratio method, allows to incorporate the spectral shape of R_{rs} in our retrievals of CDOM absorption magnitude and spectral slope coefficient. One of the main challenges for nearshore ocean color retrievals is resolving the contributions of CDOM and NAP to estimates of total in-water absorption (a_t), because of the similar exponential absorption spectral shape of both water constituents. To assess potential interference of NAP absorption in our CDOM retrievals, we examined the correlation between the satellite-retrieved CDOM and coincident in situ measurements of NAP absorption. Measurements collected during the 2011 CBODAQ field campaign (Table 1) were used to implement our CDOM algorithm (Eq. 4) on measured in situ R_{rs} and evaluate the correlation between the retrieved parameter and in situ measurements of NAP absorption ($a_{NAP}(\lambda)$, m^{-1}). Measurements of

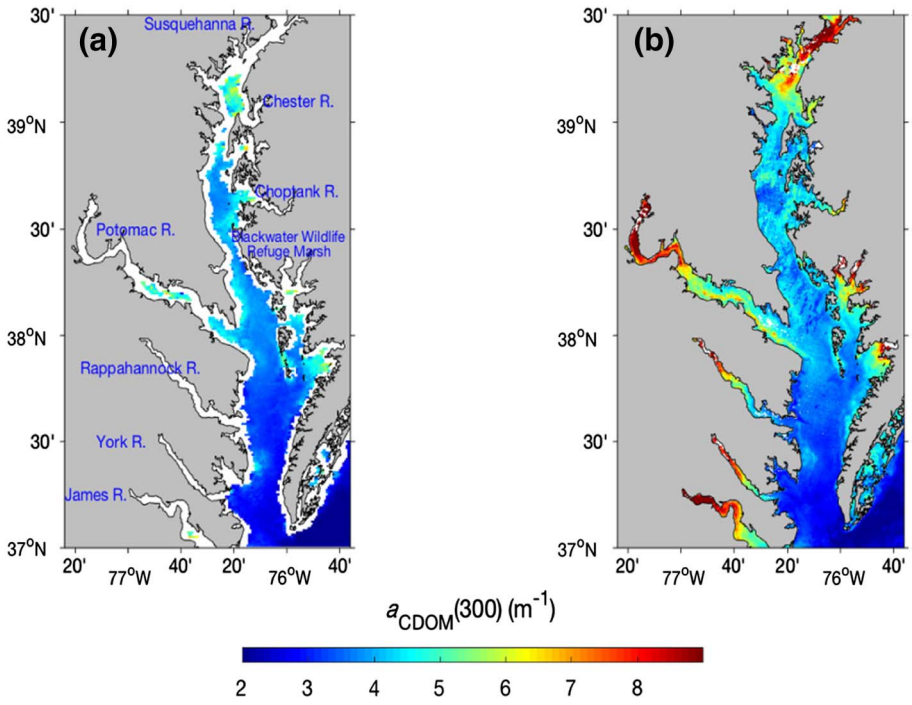

Fig. 4. Comparison of $a_{CDOM}(300)$ between (a) MODIS-A and (b) MERIS for February 2011 over the Chesapeake Bay.

a_{NAP} were only available in the 400–750 nm range, so $a_{NAP}(300)$ was calculated based on the measured $a_{NAP}(412)$ and the estimated NAP absorption spectral slope (S_{NAP}; non-linear exponential fit over 400–750 nm). S_{NAP} ranged from 0.0103 to 0.0138 nm^{-1} in the CBODAQ dataset (N = 26), consistent with previous studies (e.g., Tzortziou et al., 2007). We found that the algorithm using the functional form of Eq. (4) gave an MAPD > 100% (N = 26) between the algorithm-derived parameter and $a_{NAP}(300)$, and thus is not a good predictor of NAP dynamics. Consistent with these results, we did not find any strong correlation between a_{NAP} and the error in the CDOM retrieval (satellite-retrieved minus measured CDOM absorption) (R^2 value of 0.19 (N = 26) driven mostly by three points with the highest error; when these were excluded R^2 decreased to 0.007 (N = 23)). These results suggest that NAP amount does not have a large impact on our CDOM algorithm.

Although CDOM and NAP have a similar impact on total in-water absorption, and thus their contribution to a_t is not easy to resolve, their impact on R_{rs} is very different due to the NAP backscattering that also shows an inverse relationship with wavelength (e.g., Reynolds et al., 2001). Because of the incorporation of R_{rs}, rather than a_t, spectral shape in our MLR CDOM algorithm, the retrieval is not as sensitive to NAP variability. It should be noted that although our training and evaluation datasets included a large number of samples collected across different seasons and years, across salinity gradients and multiple estuarine-coastal environments and were, thus, representative of a range of in-water bio-optical conditions, the empirically based CDOM and $S_{275–295}$ algorithms may underperform in waters characterized by optical properties that are not captured in the training dataset (see detailed discussions in Cao and Miller, 2015).

Comparisons with in situ data demonstrated that our DOC algorithm was applicable across all seasons and study areas without requiring regional tuning or temporally specific parameterizations. This broad applicability was due, in part, to the algorithm being based on the strong relationship between $a_{CDOM}^*(300)$ and $S_{275–295}$, optical properties that both depend on the quality (e.g., chemical composition and molecular structure) of DOM, but not its amount, and have both been proposed as good tracers of DOM molecular size, aromaticity, and extent of photochemical and microbial transformations (e.g., Chin et al., 1994; Del Vecchio and Blough, 2004; Tzortziou et al., 2008). Therefore, seasonal and regional variability in the DOC versus a_{CDOM} relationship has been accounted for in our algorithms by incorporating information on the variability in $S_{275–295}$. A number of studies have demonstrated that $S_{275–295}$ is an excellent indicator of DOC-normalized CDOM absorption across seasons in nearshore environments (Fichot and Benner, 2011; Vantrepotte et al., 2015; Mannino et al., 2016; Yu et al., 2016). Similar to these studies, we found a strong relationship between $S_{275–295}$ and $a_{CDOM}^*(\lambda)$ across the northern Gulf of Mexico, the Chesapeake Bay, and the Delaware Bay waters (Fig. 2(a)–(b)). In our training dataset, the highest $a_{CDOM}^*(300)$ of 390 L mol^{-1} cm^{-1} was measured in waters draining a tidal brackish wetland during low tide in the Chesapeake Bay estuary. This CDOM sample also showed the lowest $S_{275–295}$ (0.0174 nm^{-1}), suggesting highly aromatic, highly absorbing, and high molecular weight DOM, as expected for organic matter exported from tidal marshes (Tzortziou et al., 2008). The lowest $a_{CDOM}^*(300)$ in our dataset (25 L mol^{-1} cm^{-1}) had also the highest $S_{275–295}$ (0.0478 nm^{-1}) and was measured in higher salinity, offshore waters. Our training dataset included samples from multiple years and seasons. Although DOC, a_{CDOM}, and $S_{275–295}$ all exhibited variability due to seasonal changes in CDOM source and transformations, the $S_{275–295}$ versus $a_{CDOM}^*(300)$, or similarly $a_{CDOM}^*(355)$, relationship remained remarkably tight leading to a more general and robust retrieval approach for DOC concentrations in different estuarine-coastal systems and across a range of in-water conditions.

On the other hand, the exponential decrease of $a_{CDOM}^*(300)$ with increasing $S_{275–295}$ shows little correlation between the two quantities in open-ocean environments, especially in waters with $S_{275–295}$ > 0.04 nm^{-1}, where $a_{CDOM}^*(300)$ is already very low and appears to vary slightly as $S_{275–295}$ continues to increase (Fig. 2(a)–(b)). Furthermore, the exponential nature of the relationship between $a_{CDOM}^*(300)$ and $S_{275–295}$ means that the algorithm presented in Eq. (6a) will be very sensitive to uncertainties in $S_{275–295}$ at the most nearshore locations, where $S_{275–295}$ is low and $a_{CDOM}^*(300)$ is high.

4.3. Spatial and temporal distributions of CDOM and DOC in the Chesapeake Bay

4.3.1. Spatial resolution of satellite imagery

The benefits of using a 300-m spatial resolution in the Chesapeake

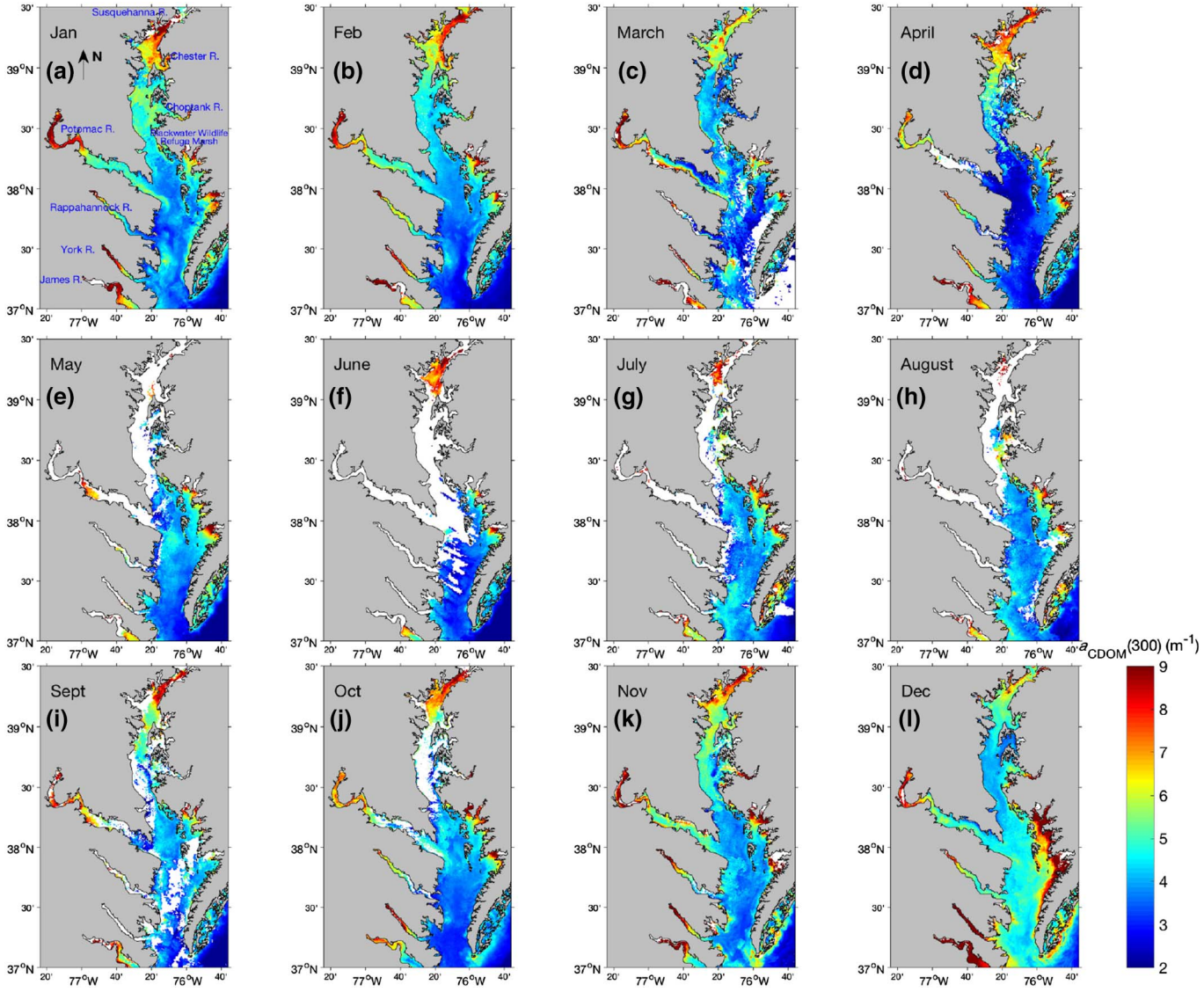

Fig. 5. MERIS monthly composites of the distribution of $a_{CDOM}(300)$ in the Chesapeake Bay and adjacent coastal waters in 2009.

Bay were demonstrated by comparing a monthly composite of $a_{CDOM}(300)$ derived from MODIS (1-km resolution at nadir) to one derived from MERIS (300 m resolution) for the month of February 2011 (Fig. 4). Both sensors captured the decrease in CDOM absorption from the upper bay to the lower bay and bay mouth. However, MODIS significantly underestimated CDOM in the upper part of the Bay. Average $a_{CDOM}(300)$ from MODIS was $\sim 5.03\ m^{-1}$, compared to $\sim 7.11\ m^{-1}$ from MERIS, for the same region within 39°10′ N to 39°15′ N latitude and 76°18′ W to 76°21′ W longitude where valid pixels from both sensors were available (Fig. 4). This is consistent with previous studies showing that lower resolution MODIS retrievals are not necessarily the arithmetic or geometric mean of higher resolution observations (Lee et al., 2012).

In addition, due to its coarse spatial resolution, after applying the NASA standard flags that are used to produce Level-3 global data products (Robinson et al., 2003) Level-3 MODIS imagery failed to capture the strong gradients in DOC and CDOM near the shoreline, such as near the mouth of the Susquehanna River or the sub-estuaries and tributaries along the western and eastern Bay shores. The maximum $a_{CDOM}(300)$ observed by MODIS was $\sim 6\ m^{-1}$ in the upper Bay, while the higher spatial resolution MERIS captured CDOM values of $> 9\ m^{-1}$ closer to the shore, at the mouth of the Susquehanna, Patuxent, York, and Choptank Rivers as well as near large wetland areas such as the Blackwater refuge marshes. Capturing these strong spatial gradients across terrestrial-aquatic margins is critical for understanding the quality, transformation, and fate of terrestrial organic matter and its impact on estuarine metabolism, ecosystem functioning, and coastal carbon budgets. These results highlight the need for high spatial resolution satellite ocean color sensors in order to capture bio-optical changes and physicobiogeochemical transformations occurring at the land–water interface.

4.3.2. Spatial and temporal patterns in estuarine CDOM and DOC

Substantial spatial variability in $a_{CDOM}(300)$, $S_{275-295}$, and DOC was observed in the MERIS monthly composites in Chesapeake Bay in 2009 (Figs. 5–7). Nearshore areas, heavily impacted by river runoff, wetland DOM export, and tidal resuspension (e.g., porewater DOM release; Boss et al., 2001), had consistently higher $a_{CDOM}(300)$ and DOC, and lower $S_{275-295}$ throughout the year, relative to the main stem of the bay. The upper Chesapeake Bay is strongly affected by the Susquehanna River discharge and was consistently characterized by high $a_{CDOM}(300)$ and also low $S_{275-295}$, which is indicative of high molecular weight and aromatic humic compounds. Near the mouth of the bay, however, monthly averages of $a_{CDOM}(300)$ decreased to 2–4 m^{-1} and DOC concentrations were below 200 $\mu mol\ L^{-1}$, while $S_{275-295}$ increased to $> 0.024\ nm^{-1}$ throughout the year, suggesting a decrease in aromaticity

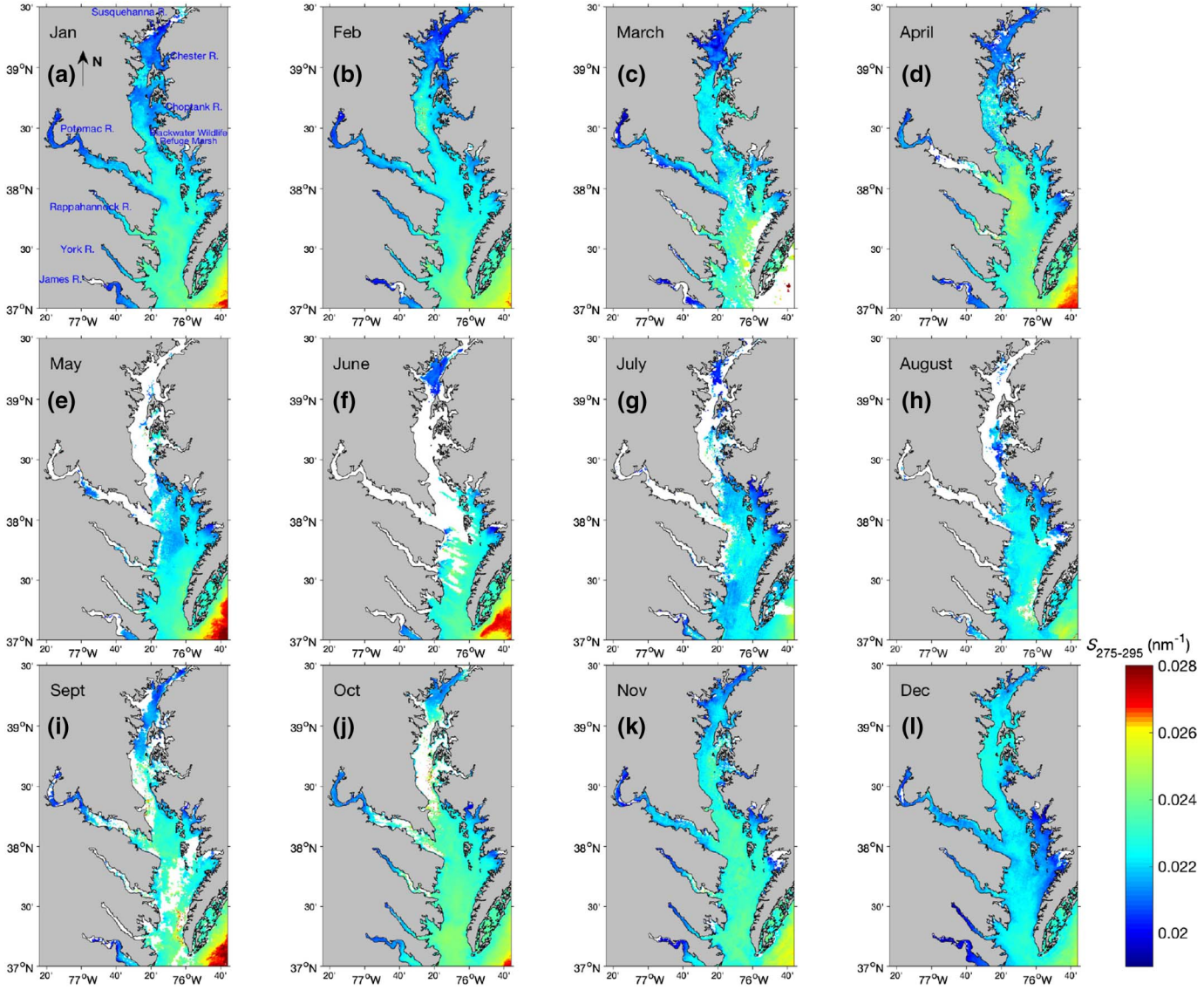

Fig. 6. Same as Fig. 5, for $S_{275–295}$.

and molecular weight, consistent with mixing as well as enhanced photochemical and microbial degradation of terrestrial DOM during transport to the coastal ocean (Helms et al., 2008). These ranges of CDOM and DOC values, and their distribution in the Bay and the mouth to the Mid-Atlantic Bight, are in good agreement with field data reported in Del Vecchio and Blough (2004) and Rochelle-Newall and Fisher (2002), suggesting reasonable performance of these algorithms across the entire bay. Rochelle-Newall and Fisher (2002) reported that DOC ranged from 249 μmol L^{-1} in the upper part of the Chesapeake Bay estuary (39°N) to 138 μmol L^{-1} in the mouth of the Chesapeake Bay during measurements in 1994 to 1997. Del Vecchio and Blough (2004) reported DOC values of approx. 300 μmol L^{-1} in the Susquehanna River mouth.

Superimposed on these spatial gradients, DOM quantity and quality also showed some seasonal variability. Inputs of terrestrial DOM from tributaries and especially the Susquehanna River were evident throughout the year but were more pronounced during Fall (September–November) with relatively high $a_{CDOM}(300)$ ($> 8\ m^{-1}$), low $S_{275–295}$ ($< 0.025\ nm^{-1}$), and elevated DOC (> 270 μmol L^{-1}) as a result of a rainy season in late 2009 (Figs. 5–7(i–l)). This influence persisted until winter due to the relatively long water residence time of ~3 to 6 months in the Bay (Kemp et al., 2005), and was indicated by elevated DOC (200–250 μmol L^{-1}) in the main stem of the Bay in December 2009. In addition to elevated water discharge, $a_{CDOM}(300)$ and DOC were both elevated (with $a_{CDOM}(300) > 12\ m^{-1}$ and DOC > 500 μmol L^{-1}, respectively) near the Eastern Shore tidal wetlands in December 2009 relative to other months, which is discussed in more detail in Section 4.4. Variability of CDOM and DOC was less discernable in the middle bay in early 2009, with moderate $a_{CDOM}(300)$ in the range of 3–4 m^{-1} from January to August in the main stem (Fig. 5(a–h)), despite strong seasonal variability in phytoplankton biomass and primary production (Son et al., 2014). This de-coupling between CDOM and chlorophyll *a* and primary production likely suggests that phytoplankton is not necessarily a major direct source of CDOM in this system, as previously shown in field studies by Rochelle-Newall and Fisher (2002).

4.3.3. *Extreme weather events*

The passage of Tropical Storm Lee over the Chesapeake Bay area in fall 2011 provides a good opportunity to demonstrate the ocean color algorithms' ability to capture changes in CDOM dynamics and DOC fluxes during extreme weather events.

Developed on September 1st 2011 over the Gulf of Mexico, Tropical Storm Lee moved north and eastward, causing extensive flooding and

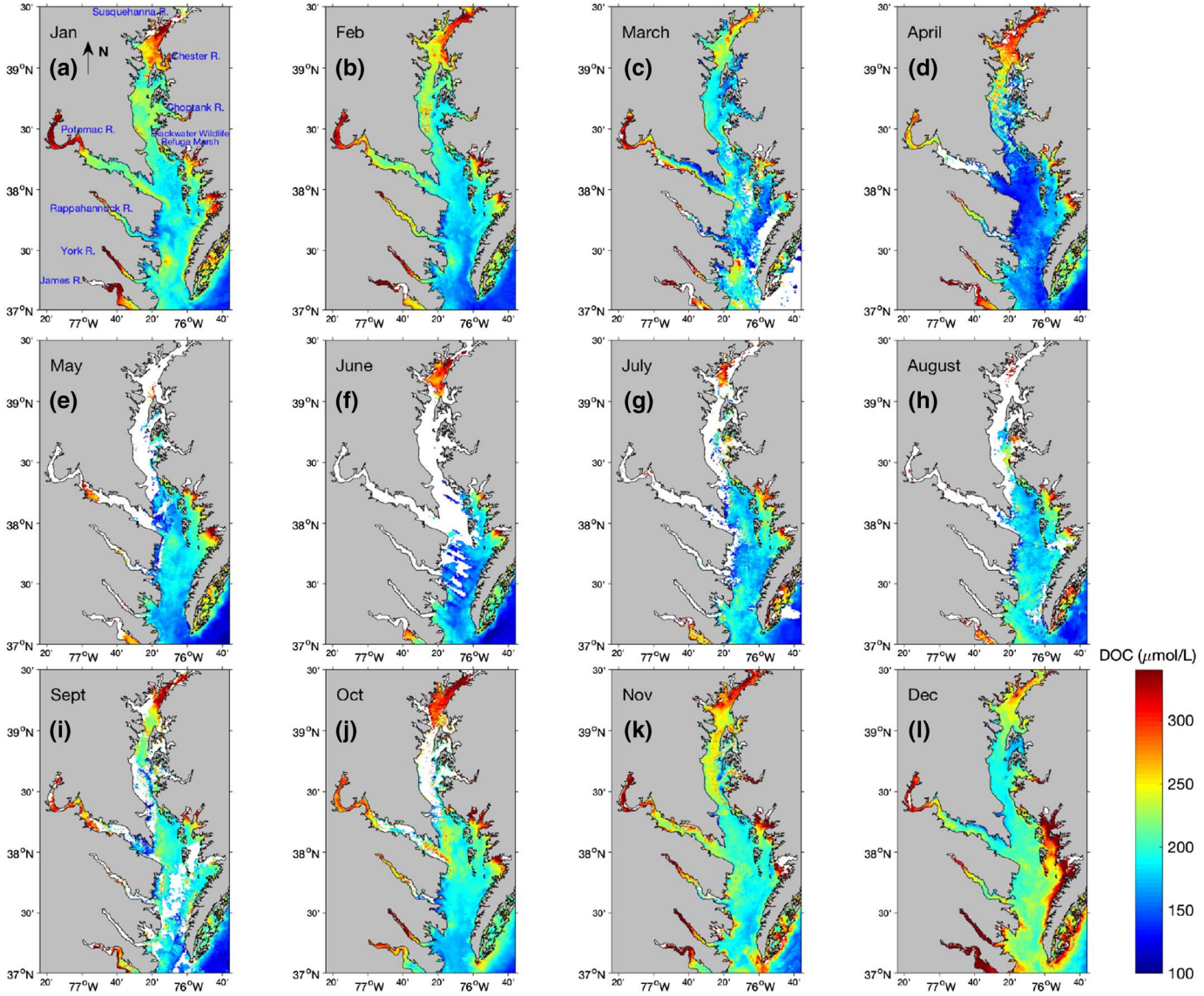

Fig. 7. Same as Fig. 5, for DOC.

transport of terrestrial materials into the Susquehanna River. After the storm passed, turbid plumes with increased total suspended material were discernable from satellite observations (http://earthobservatory.nasa.gov/IOTD/view.php?id=52169). Water discharge carried > 50 mg/L of suspended materials into the Chesapeake Bay following the storm (Fig. 5 in Aurin et al., 2013), compared to a baseline value of < 15 mg/L in 2009 (Fig. 13 in Ondrusek et al., 2012), and would also be expected to increase CDOM and DOC concentrations considerably. Implementation of our algorithms to full resolution MERIS imagery from October 2011 showed, indeed, strikingly higher $a_{CDOM}(300)$, as high as 13 m^{-1}, and a relatively lower $S_{275–295}$ of 0.0186 nm^{-1} in the upper Bay (Figs. 8(a), (b)). DOC concentration increased to 450 μmol L^{-1} (Fig. 8(c)) in remarkably good agreement with in-situ water quality monitoring in the Susquehanna River that recorded levels of DOC as high as 425 μmol L^{-1} at Conowingo Dam in the aftermath of the storm (http://data.chesapeakebay.net/ Water Quality). Comparisons between satellite retrievals during the storm event (i.e., October 2011 composite) and a baseline condition (i.e., monthly composite of October 2009, Figs. 5–7) showed large changes in DOM quality as well as quantity, with differences as large as 100% for DOC in certain areas of the Bay (Fig. 8(c)–(d)). Although CDOM and DOC were particularly high in the Susquehanna River mouth and tributaries, the influence of the storm affected DOM throughout the entire estuary.

4.4. Tidal effects on ocean color retrievals at marsh–estuary interfaces

Tidal cycles exert significant influence on the physicochemical and bio-optical properties of nearshore waters (Shi et al., 2011). In coastal areas dominated by tidal wetlands, consistent export of DOM from the wetland to the estuary and, most often, import of particulate organic matter can result in changes by a factor of 3, or more, in CDOM absorption and chlorophyll concentrations over a period of < 6 h (Tzortziou et al., 2011; Tzortziou et al., 2008). However, the impact of this strong variability over short tidal timescales on coastal ocean color retrievals is often neglected, which can have important implications not only for coastal ocean color algorithm development but also for applications of ocean color imagery to coastal carbon cycling studies. In the Chesapeake Bay, tidal marshes cover a large area (about 700 km^2) along the western and eastern Bay shores and examining the impact of tidal stage on satellite ocean color retrievals is imperative.

Located along the eastern shore, the Blackwater National Wildlife Refuge wetland is the largest marsh system in the Chesapeake Bay (Fig. 9(a)). The McCreadys Creek is one of the creeks draining these

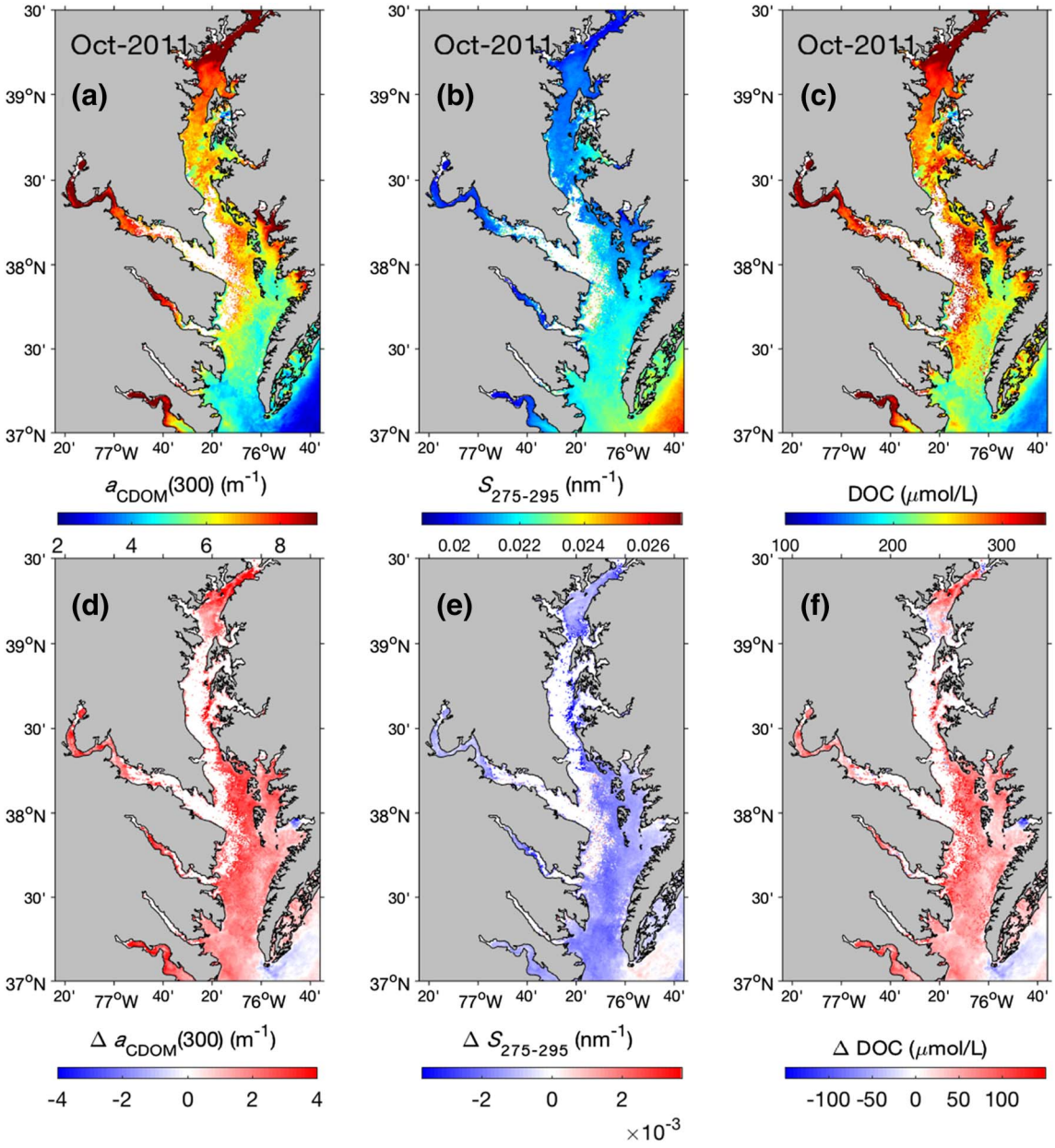

Fig. 8. (a)–(c) CDOM optical properties and DOC in the Chesapeake Bay derived from MERIS in October 2011, after the passage of Tropical Storm Lee. (d)–(f) Differences in CDOM optical properties and DOC between October 2011 (influenced by extreme precipitation) and October 2009 (not influenced by extreme weather event).

marshes into the Fishing Bay, where marsh-exported DOM merges with inputs of terrestrial (marsh, forested, and anthropogenic) materials from the Nanticoke and Wicomico Rivers. We examined the tidal stage during each individual MERIS image that was used to produce the monthly composites of satellite CDOM and DOC in December 2009, a month when our satellite retrievals showed particularly high CDOM absorption and DOC in that region of the estuary (Figs. 5(l) and 7(l)). We found that four out of the five MERIS images were sampled at, or near, low tide when water was draining the marsh exporting strongly absorbing, carbon-rich DOM to the estuary (Fig. 9(b)). Estimated DOC values were higher than 600 μmol L^{-1} near the wetlands on the low tide satellite images (Fig. 9(c)), compared to DOC values of ~350 μmol L^{-1} at high tide (Fig. 9(d)). CDOM and DOC were also particularly high in the mouth of the Nanticoke and Wicomico Rivers at the low tide images, as expected due to the export of strongly absorbing terrestrial DOM; however, the Blackwater marsh export had a stronger influence on nearshore CDOM and DOC gradients. These results are consistent with field observations in Chesapeake Bay estuarine waters adjacent to tidal marshes showing changes in DOC by a factor of two between low and high tide (Tzortziou et al., 2008).

The data presented in Fig. 9 illustrates that MERIS/MODIS imagery in tidally influenced nearshore waters gets inevitably collected at random tidal stages and can potentially lead to important biases in binned satellite CDOM and DOC products, with composites dominated by low tide (high tide) scenes overestimating (underestimating) carbon stocks in nearshore environments. Multi-image binned products of particulate matter will also be affected, but in different ways across different systems. In nearshore waters dominated by riverine fluxes, particulate matter is expected to be higher in ebbing tides. On the contrary, previous studies in tidal wetlands have shown an import (i.e., removal) of chlorophyll *a* and other particulate organic carbon by wetlands at ebbing tide (Osburn et al., 2015; Tzortziou et al., 2011). Assimilating satellite ocean color products into biogeochemical or hydrodynamic models without considering tidal stages can lead to large uncertainties in carbon fluxes and budgets for coastal zones. Moreover, differences in the distribution of individual overpasses across the tidal

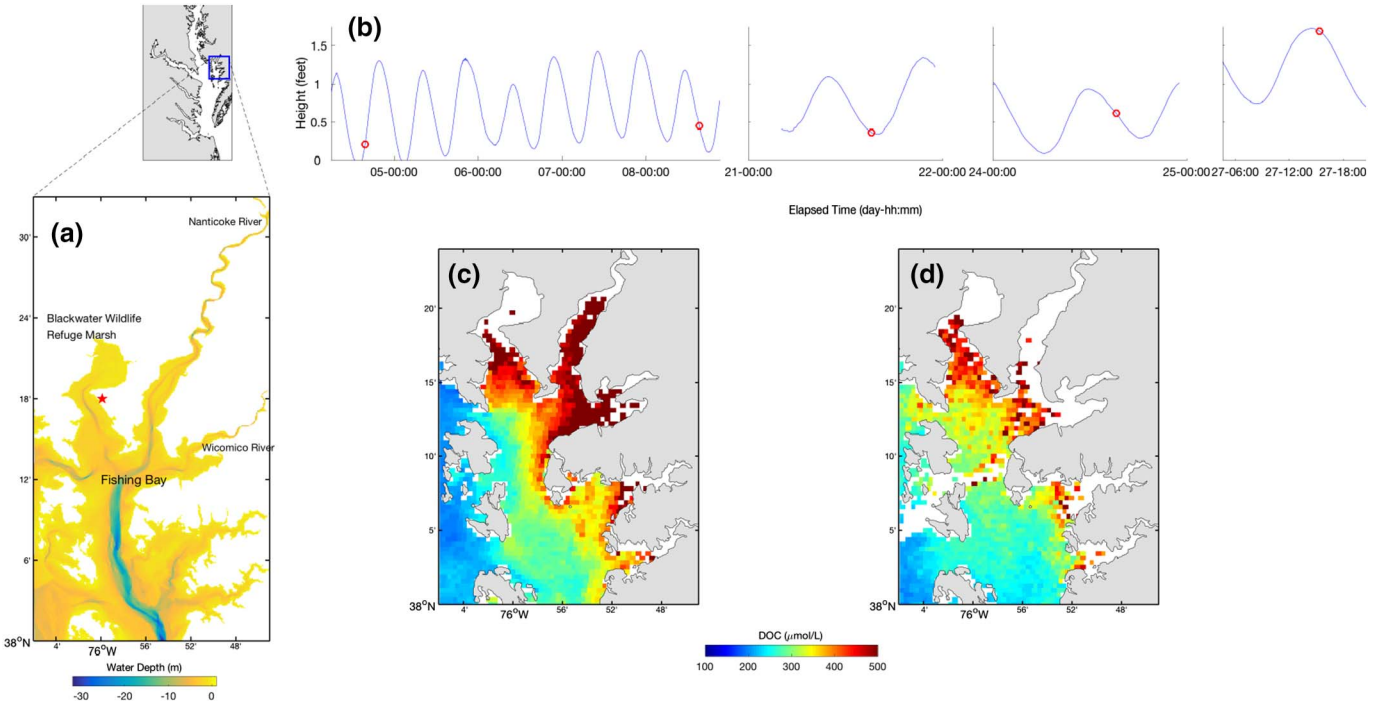

Fig. 9. (a) Area of interest for examining tidal influence on CDOM and DOC dynamics in estuarine waters adjacent to the Blackwater National Wildlife Refuge marshes. (b) Tidal height, as monitored at the McCreadys Creek, Maryland (indicated by a red star on Fig. 9(a), NOAA tidal station ID: 8571559). Red circles mark the satellite overpass time of each individual MERIS image used to produce the monthly composites. MERIS retrieved DOC concentration during (c) the four low tides and (d) the one high tide scenes in December 2009.

cycle can result in false seasonal patterns when monthly satellite ocean color composites are used for assessing seasonal variability in nearshore waters. Therefore, we recommend that information on tidal stage is taken into account when interpreting composite satellite images in tidally influenced nearshore waters.

Although the MERIS 300-m resolution data provide improved coverage of the land–ocean interface, its fairly long sensor revisit time (~3 days at the Chesapeake Bay latitude) still poses a challenge for resolving sub-daily tidal dynamics. Indeed, all coastal systems under strong tidal influence face similar problems of a lack of frequent and valid satellite observations due to cloud cover and other factors. Recent studies using MODIS imagery showed that the odds of obtaining cloud-free observations in Chesapeake Bay are only 30% (Feng et al., 2016), and of these 30% cloud-free observations only a small portion (~15%) can provide valid ocean color retrievals (Feng and Hu, 2016). This poses a significant challenge in using polar-orbiting satellites to quantify biogeochemical exchanges and highly dynamic physical and biological processes in estuarine and coastal waters. Sensors on geostationary platforms can help address this challenge by observing coastal ecosystems at sufficient temporal and spatial scales to resolve nearshore processes, such as tides, and track carbon pools and pollutants (Fishman et al., 2012).

5. Conclusions

New remote sensing algorithms were developed for retrieving CDOM quality and DOC dynamics across estuarine–coastal systems using a multiple linear regression approach. Because of the incorporation of the R_{rs}, rather than a_t, spectral shape in our MLR CDOM algorithm, we showed that the retrieval is not sensitive to NAP variability. DOC concentration was retrieved based on a tight relationship between the DOC-specific CDOM absorption, $a_{CDOM}^*(\lambda)$, and the CDOM spectral slope, $S_{275–295}$, two parameters that both depend only on the CDOM quality and have been shown to be strongly inversely correlated across coastal systems and environmental conditions. This approach allowed to overcome the seasonal dependence of conventional a_{CDOM}-to-DOC algorithms and resulted in very good algorithm performance across spatial and temporal scales. Algorithm evaluation using satellite R_{rs} resulted in relative errors (MAPD) for $a_{CDOM}(300)$, $S_{275–295}$, and DOC retrievals of 36% (N = 44), 8.8% (N = 44), and 33% (N = 53), respectively, for MODIS-A, and 29% (N = 17), 9.5% (N = 14), and 18% (N = 32), respectively, for MERIS. These relative errors are comparable to those previously reported for satellite retrievals of CDOM and DOC products in less optically complex, further offshore waters. One of the advantages of using more generalized algorithms, such as the ones discussed here, is that these algorithms can be used to capture variability not only across a larger spatial domain or multiple systems but, more generally, across a wider range of conditions even within a smaller region, or within the same estuary. Indeed, applying these algorithms to full resolution MERIS satellite imagery over the Chesapeake Bay estuary captured spatial gradients, seasonal variability, and year-to-year changes in CDOM quality and DOC concentrations associated with riverine inputs, wetland carbon export, and the passage of tropical storm Lee over this region in October 2011.

Application of these algorithms to MERIS imagery over the smaller, but strongly inhomogeneous, spatial domain of the Blackwater Refuge wetland-estuary interface, captured the strong spatial and temporal variability in CDOM and DOC associated with tidal biogeochemical exchanges, consistent with field observations. These results highlighted that tides have a strong influence on retrievals of carbon distribution and dynamics from ocean color observations. While Level-3 binned data products are a powerful tool for exploring large scale processes at global scale, binning multiple satellite images results in unknown contributions of low-tide versus high-tide scenes, which is problematic in highly dynamic nearshore environments. Integrating multi-day binned ocean color products into numerical models should be done with caution for tidally influenced coastal zones. This is particularly important for remote sensing retrievals using higher spatial resolution satellite imagery, such as Landsat 8 and Sentinel-2/MSI observations, that can capture small scale processes in nearshore environments.

Our findings highlight that high spatial resolution multi-spectral observations, similar to or better than the full resolution MERIS, are

critical for resolving biogeochemical processes in estuarine-coastal systems from space. At the same time, high temporal resolution (1–3 h) ocean color observations, for example from a geostationary platform, are necessary for capturing highly dynamic diurnal processes and biogeochemical exchanges in estuaries and their margins. These advanced remote sensing tools are urgently needed for monitoring and understanding the resilience, responses, and feedbacks of estuarine and coastal ecosystems to ongoing anthropogenic disturbances and global environmental change.

Acknowledgements

Various NASA programs supported the work described in this manuscript (Carbon Cycle Synthesis project NNX14AM37G, Carbon Cycle Science Program project NNX14AP06G, Interdisciplinary Science Program project NNX14AF93G; and NASA-funded CBODAQ and GoMEX field campaigns). Support was also provided by NSF projects OCE0443263 and DEB1556556. We thank the Editor and three anonymous reviewers for their constructive comments. We would like to thank Matteo Ottaviani, Sean Bailey, Norman Kuring, Don Shea, and George White for providing feedback on the processing of the satellite data. We thank Steven Lohrenz and Ronald Benner for access to the CDOM, DOC, and R_{rs} data from the GulfCarbon project funded by NSF grants OCE-0752254 and OCE-0850653. We are grateful to the scientists who contributed bio-optical data to the SeaBASS database, and to the NASA Goddard Space Flight Center Ocean Biology Processing Group for their efforts in providing high quality satellite ocean color data.

References

Adolf, J.E., Yeager, C.L., Miller, W.D., Mallonee, M.E., Harding, L.W., 2006. Environmental forcing of phytoplankton floral composition, biomass, and primary productivity in Chesapeake Bay, USA. Estuar. Coast. Shelf Sci. 67, 108–122.

Ahmad, Z., McClain, C.R., Herman, J.R., Franz, B., Kwiatkowska, E., Robinson, W., Bucsela, E.J., Tzortziou, M., 2007. Atmospheric correction for NO2 absorption in retrieving water-leaving reflectances from the SeaWiFS and MODIS measurements. Appl. Opt. 46 (26). http://dx.doi.org/10.1364/AO.46.006504.

Asmala, E., Stedmon, C.A., Thomas, D.N., 2012. Linking CDOM spectral absorption to dissolved organic carbon concentrations and loadings in boreal estuaries. Estuar. Coast. Shelf Sci. 111, 107–117.

Aurin, D., Mannino, A., Franz, B., 2013. Spatially resolving ocean color and sediment dispersion in river plumes, coastal systems, and continental shelf waters. Remote Sens. Environ. 137, 212–225.

Bailey, S.W., Werdell, P.J., 2006. A multi-sensor approach for the on-orbit validation of ocean color satellite data products. Remote Sens. Environ. 102, 12–23.

Bailey, S.W., Franz, B.A., Werdell, P.J., 2010. Estimation of near-infrared water-leaving reflectancefor satellite ocean color data processing. Opt. Express 18, 7521–7527.

Balch, W., et al., 2016. Toward a quantitative and empirical dissolved organic carbon budget for the Gulf of Maine, a semienclosed shelf sea. Glob. Biogeochem. Cycles 30 (2), 268–292.

Bates, N.R., Hansell, D.A., 1999. A high resolution study of surface layer hydrographic and biogeochemical properties between Chesapeake Bay and Bermuda. Mar. Chem. 67, 1–16.

Bauer, J.E., Cai, W.J., Raymond, P.A., Bianchi, T.S., Hopkinson, C.S., Regnier, P.A.G., 2013. The changing carbon cycle of the coastal ocean. Nature 504, 61–70.

Belzile, C., Guo, L., 2006. Optical properties of low molecular weight and colloidal organic matter: application of the ultrafiltration permeation model to DOM absorption and fluorescence. Mar. Chem. 98, 183–196.

Benner, R., 2002. Chemical composition and reactivity. In: Biogeochemistry of marine dissolved organic matter. 3. pp. 56–90.

Boss, E., Pegau, W.S., Zaneveld, J.R.V., Barnard, A.H., 2001. Spatial and temporal variability of absorption by dissolved material at a continental shelf. J. Geophys. Res. 106 (C5), 9499–9507.

Bowers, D.G., Evans, D., Thomas, D.N., Ellis, K., Williams, P.J.B., 2004. Interpreting the colour of an estuary. Estuar. Coast. Shelf Sci. 59, 13–20.

Bronk, D.A., 2002. Dynamics of DON. In: Biogeochemistry of marine dissolved organic matter. 384. pp. 153–247.

Cao, F., Miller, W.L., 2015. A new algorithm to retrieve chromophoric dissolved organic matter (CDOM) absorption spectra in the UV from ocean color. J. Geophys. Res. Oceans 120, 496–516.

Carder, K.L., Chen, F.R., Lee, Z.P., Hawes, S.K., Kamykowski, D., 1999. Semianalytic moderate-resolution imaging spectrometer algorithms for chlorophyll a and absorption with bio-optical domains based on nitrate-depletion temperatures. J. Geophys. Res. Oceans 104, 5403–5421.

Carlson, C.A., 2002. Production and removal processes. In: Biogeochemistry of Marine Dissolved Organic Matter, pp. 91–151.

Cauwet, G., 2002. DOM in the coastal zone. In: Biogeochemistry Of Marine Dissolved Organic Matter, pp. 579–609.

Chin, Y.-P., Aiken, G., O'Loughlin, E., 1994. Molecular weight, polydispersity, and spectroscopic properties of aquatic humic substances. Environ. Sci. Technol. 28, 1853–1858.

Das, A., Justic, D., Inoue, M., Hoda, A., Huang, H., Park, D., 2012. Impacts of Mississippi River diversions on salinity gradients in a deltaic Louisiana estuary: ecological and management implications. Estuar. Coast. Shelf Sci. 111, 17–26.

Del Castillo, C.E., Miller, R.L., 2008. On the use of ocean color remote sensing to measure the transport of dissolved organic carbon by the Mississippi River Plume. Remote Sens. Environ. 112, 836–844.

Del Castillo, C.E., Coble, P.G., Morell, J.M., Lopez, J.M., Corredor, J.E., 1999. Analysis of the optical properties of the Orinoco River plume by absorption and fluorescence spectroscopy. Mar. Chem. 66, 35–51.

Del Vecchio, R., Blough, N.V., 2004. Spatial and seasonal distribution of chromophoric dissolved organic matter and dissolved organic carbon in the Middle Atlantic Bight. Mar. Chem. 89, 169–187.

Dong, Q., Shaoling, S., Zhongping, L., 2013. An algorithm to retrieve absorption coefficient of chromophoric dissolved organic matter from ocean color. Remote Sens. Environ. 128, 259–267. http://dx.doi.org/10.1016/j.rse.2012.10.013.

Feng, L., Hu, C., 2016. Comparison of Valid Ocean observations between MODIS Terra and Aqua over the global oceans. IEEE Trans. Geosci. Remote Sens. 54, 1575–1585.

Feng, L., Hu, C., Barnes, B., Mannino, A., Heidinger, A.K., Strabala, K., et al., 2016. Cloud and sun-glint statistics derived from GOES and MODIS observations over the Intra-Americas Sea for GEO-CAPE mission planning. J. Geophys. Res. Atmos. 122, 1725–1745.

Fichot, C.G., Benner, R., 2011. A novel method to estimate DOC concentrations from CDOM absorption coefficients in coastal waters. Geophys. Res. Lett. 38.

Fichot, C.G., Benner, R., 2012. The spectral slope coefficient of chromophoric dissolved organic matter (S275–295) as a tracer of terrigenous dissolved organic carbon in river-influenced ocean margins. Limnol. Oceanogr. 57, 1453–1466.

Fichot, C.G., Lohrenz, S.E., Benner, R., 2014. Pulsed, cross-shelf export of terrigenous dissolved organic carbon to the Gulf of Mexico. J. Geophys. Res. Oceans 119, 1176–1194.

Fishman, J., Iraci, L.T., Al-Saadi, J., Chance, K., Chavez, F., Chin, M., et al., 2012. The United States' next generation of atmospheric composition and coastal ecosystem measurements: NASA's geostationary coastal and air pollution events (GEO-CAPE) mission. Bull. Am. Meteorol. Soc. 93, 1547–1566.

Gibson, J.R., Najjar, R.G., 2000. The response of Chesapeake Bay salinity to climate-induced changes in streamflow. Limnol. Oceanogr. 45, 1764–1772.

Goyens, C., Jamet, C., Schroeder, T., 2013. Evaluation of four atmospheric correction algorithms for MODIS-Aqua images over contrasted coastal waters. Remote Sens. Environ. 131, 63–75.

Green, S.A., Blough, N.V., 1994. Optical absorption and fluorescence properties of chromophoric dissolved organic matter in natural waters. Limnol. Oceanogr. 39, 1903–1916.

Guéguen, C., Mokhtar, M., Perroud, A., McCullough, G., Papakyriakou, T., 2016. Mixing and photoreactivity of dissolved organic matter in the Nelson/Hayes estuarine system (Hudson Bay, Canada). J. Mar. Syst. 161, 42–48. http://dx.doi.org/10.1016/j.jmarsys.2016.05.005.

Harding, L.W., 1994. Long-term trends in the distribution of phytoplankton in Chesapeake Bay: roles of light, nutrients and streamflow. Mar. Ecol. Prog. Ser. 104, 267–291.

Harvey, H.R., Mannino, A., 2001. The chemical composition and cycling of particulate and macromolecular dissolved organic matter in temperate estuaries as revealed by molecular organic tracers. Org. Geochem. 32, 527–542.

Hedges, J.I., 1992. Global biogeochemical cycles: progress and problems. Mar. Chem. 39, 67–93.

Helms, J.R., Stubbins, A., Ritchie, J.D., Minor, E.C., Kieber, D.J., Mopper, K., 2008. Absorption spectral slopes and slope ratios as indicators of molecular weight, source, and photobleaching of chromophoric dissolved organic matter. Limnol. Oceanogr. 53, 955–969.

Herrmann, M., Najjar, R.G., Kemp, W.G., Alexander, R.B., Boyer, E.W., Cai, W.J., et al., 2015. Net ecosystem production and organic carbon balance of US East Coast estuaries: a synthesis approach. Glob. Biogeochem. Cycles 29, 96–111.

Hood, R.R., Wang, H.V., Purcell, J.E., Houde, E.D., Harding Jr., L.W., 1999. Modeling particles and pelagic organisms in Chesapeake Bay: convergent features control plankton distributions. J. Geophys. Res. All Series 104, 1223–1244.

Hu, C., Carder, K.L., Muller-Karger, F.E., 2001. How precise are SeaWiFS ocean color estimates? Implications of digitization-noise errors. Remote Sens. Environ. 76, 239–249.

Joshi, I.D., et al., 2017. Assessing chromophoric dissolved organic matter (CDOM) distribution, stocks, and fluxes in Apalachicola Bay using combined field, VIIRS ocean color, and model observations. Remote Sens. Environ. 191, 359–372.

Kahru, M., Mitchell, B.G., 2001. Seasonal and non-seasonal variability of satellite-derived chlorophyll and colored dissolved organic matter concentration in the California Current. J. Geophys. Res. 106, 2517–2529.

Kemp, W.M., Boynton, W.R., Adolf, J.E., Boesch, D.F., Boicourt, W.C., Brush, G., et al., 2005. Eutrophication of Chesapeake Bay: historical trends and ecological interactions. Mar. Ecol. Prog. Ser. 303, 1–29.

Kemp, G.P., Day, J.W., Freeman, A.M., 2014. Restoring the sustainability of the Mississippi River Delta. Ecol. Eng. 65, 131–146.

Le, C., Hu, C., Cannizzaro, J., Duan, H., 2013a. Long-term distribution patterns of remotely sensed water quality parameters in Chesapeake Bay. Estuar. Coast. Shelf Sci. 128, 93–103.

Le, C., Hu, C., English, D., Cannizzaro, J., Chen, Z., Kovach, et al., 2013b. Inherent and

apparent optical properties of the complex estuarine waters of Tampa Bay: what controls light? Estuar. Coast. Shelf Sci. 117, 54–69.
Le, C., Lehrter, J.C., Schaeffer, B.A., Hu, C., Murrell, M.C., Hagy, et al., 2016. Bio-optical water quality dynamics observed from MERIS in Pensacola Bay, Florida. Estuar. Coast. Shelf Sci. 173, 26–38.
Lee, Z.P., Carder, K.L., Arnone, R.A., 2002. Deriving inherent optical properties from water color: a multiband quasi-analytical algorithm for optically deep waters. Appl. Opt. 41, 5755–5772.
Lee, Z.P., Arnone, R., Hu, C., Werdell, P.J., Lubac, B., 2010. Uncertainties of optical parameters and their propagations in an analytical ocean color inversion algorithm. Appl. Opt. 49, 369–381.
Lee, Z., Hu, C., Arnone, R., Liu, Z., 2012. Impact of sub-pixel variations on ocean color remote sensing products. Opt. Express 20, 20844–20854.
Liu, Q., Pan, D., Bai, Y., Wu, K., Chen, C.T.A., Liu, Z., et al., 2014. Estimating dissolved organic carbon inventories in the East China Sea using remote-sensing data. J. Geophys. Res. Oceans 119, 6557–6574.
Lohrenz, S.E., Redalje, D.G., Cai, W.J., Acker, J., Dagg, M., 2008. A retrospective analysis of nutrients and phytoplankton productivity in the Mississippi River plume. Cont. Shelf Res. 28, 1466–1475.
Loisel, H., Vantrepotte, V., Dessailly, D., Mériaux, X., 2014. Assessment of the colored dissolved organic matter in coastal waters from ocean color remote sensing. Opt. Express 11, 13109–13124. http://dx.doi.org/10.1364/OE.22.013109.
Lunetta, R.S., Schaeffer, B.A., Stumpf, R.P., Keith, D., Jacobs, S.A., Murphy, M.S., 2015. Evaluation of cyanobacteria cell count detection derived from MERIS imagery across the eastern USA. Remote Sens. Environ. 157, 24–34.
Magnuson, A., Harding, L.W., Mallonee, M.E., Adolf, J.E., 2004. Bio-optical model for Chesapeake Bay and the middle Atlantic bight. Estuar. Coast. Shelf Sci. 61, 403–424.
Mannino, A., Harvey, H.R., 1999. Lipid composition in particulate and dissolved organic matter in the Delaware Estuary: sources and diagenetic patterns. Geochim. Cosmochim. Acta 63, 2219–2235.
Mannino, A., Rodger, H.R., 2004. Black carbon in estuarine and coastal ocean dissolved organic matter. Limnol. Oceanogr. 49, 735–740.
Mannino, A., Russ, M.E., Hooker, S.B., 2008. Algorithm development and validation for satellite-derived distributions of DOC and CDOM in the US Middle Atlantic Bight. J. Geophys. Res. Oceans 113.
Mannino, A., Novak, M.G., Hooker, S.B., Hyde, K., Aurin, D., 2014. Algorithm development and validation of CDOM properties for estuarine and continental shelf waters along the northeastern US coast. Remote Sens. Environ. 152, 576–602.
Mannino, A., Signorini, S.R., Novak, M.G., Wilkin, J., Friedrichs, M.A.M., Najjar, R.G., 2016. Dissolved organic carbon fluxes in the Middle Atlantic Bight: An integrated approach based on satellite data and ocean model products. J. Geophys. Res. Biogeosci. 121, 312–336. http://dx.doi.org/10.1002/2015JG003031.
Maritorena, S., Siegel, D.A., Peterson, A.R., 2002. Optimization of a semianalytical ocean color model for global-scale applications. Appl. Opt. 41, 2705–2714.
McIntosh, H.A., 2013. Composition, Sources, and Age of Dissolved and Particulate Organic Matter in the Delaware River and Estuary (Thesis). Virginia Institute of Marine Science.
Mélin, F., Zibordi, G., Berthon, J.F., Bailey, S., Franz, B., Voss, et al., 2011. Assessment of MERIS reflectance data as processed with SeaDAS over the European seas. Opt. Express 19, 25657–25671.
Morel, A., Gentili, B., 2009. A simple band ratio technique to quantify the colored dissolved and detrital organic material from ocean color remotely sensed data. Remote Sens. Environ. 113, 998–1011.
Mouw, C.B., Greb, S., Aurin, D., DiGiacomo, P.M., Lee, Z., Twardowski, M., et al., 2015. Aquatic color radiometry remote sensing of coastal and inland waters: challenges and recommendations for future satellite missions. Remote Sens. Environ. 160, 15–30.
Nelson, N.B., Siegel, D.A., Michaels, A.F., 1998. Seasonal dynamics of colored dissolved material in the Sargasso Sea. Deep-Sea Res. I Oceanogr. Res. Pap. 45, 931–957.
Ondrusek, M., Stengel, E., Kinkade, C.S., Vogel, R.L., Keegstra, P., Hunter, C., et al., 2012. The development of a new optical total suspended matter algorithm for the Chesapeake Bay. Remote Sens. Environ. 119, 243–254.
Osburn, C.L., Stedmon, C.A., 2011. Linking the chemical and optical properties of dissolved organic matter in the Baltic–North Sea transition zone to differentiate three allochthonous inputs. Mar. Chem. 126, 281–294.
Osburn, C.L., Mikan, M.P., Etheridge, J.R., Burchell, M.R., Birgand, F., 2015. Seasonal variation in the quality of dissolved and particulate organic matter exchanged between a salt marsh and its adjacent estuary. J. Geophys. Res. Biogeosci. 120, 1430–1449.
Osburn, C.L., Boyd, T.J., Montgomery, M.T., Bianchi, T.S., Coffin, R.B., Paerl, H.W., 2016. Optical proxies for terrestrial dissolved organic matter in estuaries and coastal waters. Front. Mar. Sci. 2, 127.
Prairie, Y.T., 2008. Carbocentric limnology: looking back, looking forward. Can. J. Fish. Aquat. Sci. 65, 543–548.
Rabalais, N.N., Turner, R.E., Wiseman Jr, W.J., 2002. Gulf of Mexico hypoxia, aka "The dead zone". Annu. Rev. Ecol. Syst. 33 (1), 235–263.
Reynolds, R.A., Stramski, D., Mitchell, B.G., 2001. A chlorophyll-dependent semi-analytical reflectance model derived from field measurements of absorption and backscattering coefficients within the Southern Ocean. J. Geophys. Res. Oceans 106, 7125–7138.
Robinson, W.D., Franz, B.A., Patt, F.S., Bailey, S.W., Werdell, P.J., 2003. Masks and flags updates. Algorithm updates for the fourth Sea-WiFS data reprocessing. NASA Tech. Memo. 206892, 34–40.
Rochelle-Newall, E.J., Fisher, T.R., 2002. Chromophoric dissolved organic matter and dissolved organic carbon in Chesapeake Bay. Mar. Chem. 77, 23–41.
Salisbury, J., Vandemark, D., Joensson, B., Balch, W., Chakraborty, S., Lohrenz, S., et al., 2015. How can present and future satellite missions support scientific studies that Address Ocean acidification? Oceanography 28, 108–121.
Sharp, J.H., Yoshiyama, K., Parker, A.E., Schwartz, M.C., Curless, S.E., Beauregard, A.Y., et al., 2009. A biogeochemical view of estuarine eutrophication: seasonal and spatial trends and correlations in the Delaware estuary. Estuar. Coasts 32, 1023–1043.
Shi, W., Wang, M., Jiang, L., 2011. Spring-neap tidal effects on satellite ocean color observations in the Bohai Sea, Yellow Sea, and East China Sea. J. Geophys. Res. Oceans 116.
Siegel, D.A., Maritorena, S., Nelson, N.B., Behrenfeld, M.J., 2005. Independence and interdependencies among global ocean color properties: reassessing the bio-optical assumption. J. Geophys. Res. Oceans 110.
Slonecker, E.T., Jones, D.K., Pellerin, B.A., 2016. The new Landsat 8 potential for remote sensing of colored dissolved organic matter (CDOM). Mar. Pollut. Bull. 107 (2), 518–527.
Son, S., Wang, M., Harding, L.W., 2014. Satellite-measured net primary production in the Chesapeake Bay. Remote Sens. Environ. 144, 109–119.
Spencer, R.G.M., Butler, K.D., Aiken, G.R., 2012. Dissolved organic carbon and chromophoric dissolved organic matter properties of rivers in the USA. J. Geophys. Res. Biogeosci. 117.
Spyrakos, E., Vilas, L.G., Palenzuela, J.M.T., Barton, E.D., 2011. Remote sensing chlorophyll a of optically complex waters (rias Baixas, NW Spain): application of a regionally specific chlorophyll a algorithm for MERIS full resolution data during an upwelling cycle. Remote Sens. Environ. 115, 2471–2485.
Stanley, E.H., Powers, S.M., Lottig, N.R., Buffam, I., Crawford, J.T., 2012. Contemporary changes in dissolved organic carbon (DOC) in human-dominated rivers: is there a role for DOC management? Freshw. Biol. 57, 26–42.
Stedmon, C.A., Markager, S., Kaas, H., 2000. Optical properties and signatures of chromophoric dissolved organic matter (CDOM) in Danish coastal waters. Estuar. Coast. Shelf Sci. 51, 267–278.
Tzortziou, M., Subramaniam, A., Herman, J.R., Gallegos, C.L., Neale, P.J., Harding, L.W., 2007. Remote sensing reflectance and inherent optical properties in the mid Chesapeake Bay. Estuar. Coast. Shelf Sci. 72, 16–32.
Tzortziou, M., Neale, P.J., Osburn, C.L., Megonigal, J.P., Maie, N., Jaffé, R., 2008. Tidal marshes as a source of optically and chemically distinctive colored dissolved organic matter in the Chesapeake Bay. Limnol. Oceanogr. 53, 148.
Tzortziou, M., Neale, P.J., Megonigal, J.P., Pow, C.L., Butterworth, M., 2011. Spatial gradients in dissolved carbon due to tidal marsh outwelling into a Chesapeake Bay estuary. Mar. Ecol. Prog. Ser. 426, 41–56.
Tzortziou, M., Herman, J.R., Ahmad, Z., Loughner, C.P., Abuhassan, N., Cede, A., 2014. Atmospheric NO2 dynamics and impact on ocean color retrievals in urban nearshore regions. J. Geophys. Res. Oceans 119, 3834–3854.
Tzortziou, M., Zeri, C., Dimitriou, E., Ding, Y., Jaffé, R., Anagnostou, E., et al., 2015. Colored dissolved organic matter dynamics and anthropogenic influences in a major transboundary river and its coastal wetland. Limnol. Oceanogr. 60, 1222–1240.
Vantrepotte, V., Danhiez, F.-P., Loisel, H., Ouillon, S., Mériaux, X., Cauvin, A., et al., 2015. CDOM-DOC relationship in contrasted coastal waters: implication for DOC retrieval from ocean color remote sensing observation. Opt. Express 23, 33–54.
Werdell, P.J., Franz, B.A., Bailey, S.W., Feldman, G.C., Boss, E., Brando, V.E., et al., 2013. Generalized ocean color inversion model for retrieving marine inherent optical properties. Appl. Opt. 52, 2019–2037.
Yu, X., Shen, F., Liu, Y., 2016. Light absorption properties of CDOM in the Changjiang (Yangtze) estuarine and coastal waters: an alternative approach for DOC estimation. Estuar. Coast. Shelf Sci. 181, 302–311.